Title:

Mycolactone causes destructive Sec61-dependent loss of the endothelial glycocalyx and vessel basement membrane: a new indirect mechanism driving tissue necrosis in *Mycobacterium ulcerans* infection

Author names and affiliations:

Louise Tzung-Harn Hsieh[1,*], Belinda S. Hall[1,*], Jane Newcombe[1], Tom A. Mendum[1], Sonia Santana-Varela[1], Yagnesh Umrania[2], Michael J. Deery[2], Wei Q. Shi[3], Josué Diaz-Delgado[4], Francisco J. Salguero[5], Rachel E Simmonds[1]

[1] Dept of Microbial Sciences, School of Bioscience and Medicine, University of Surrey

[2] Cambridge Centre for Proteomics, University of Cambridge, Cambridge, UK

[3] Department of Chemistry, Ball State University, Muncie, IN 47306, USA

[4] Texas A&M Veterinary Medical Diagnostic Laboratory, College Station, Texas, USA

[5] United Kingdom Health Security Agency. UKHSA-Porton Down, Salisbury, U.K.

* Equal contribution

Abstract

The drivers of tissue necrosis in *Mycobacterium ulcerans* infection (Buruli ulcer disease) have historically been ascribed solely to the directly cytotoxic action of the diffusible exotoxin, mycolactone. However, its role in the clinically-evident vascular component of disease aetiology remains poorly explained. We have now dissected mycolactone's effects on primary vascular endothelial cells *in vitro* and *in vivo*. We show that mycolactone-induced changes in endothelial morphology, adhesion, migration, and permeability are dependent on its action at the Sec61 translocon. Unbiased quantitative proteomics identified a profound effect on proteoglycans, driven by rapid loss of type II transmembrane proteins of the Golgi, including enzymes required for glycosaminoglycan (GAG) synthesis, combined with a reduction in the core proteins themselves. Loss of the glycocalyx is likely to be of particular mechanistic importance, since knockdown of galactosyltransferase II (beta-1,3-galactotransferase 6; B3GALT6), the GAG linker-building enzyme, phenocopied the permeability and phenotypic changes induced by mycolactone. Additionally, mycolactone depleted many secreted basement membrane components and microvascular basement membranes were disrupted *in vivo*. Remarkably, exogenous addition of laminin-511 reduced endothelial cell rounding, restored cell attachment and reversed the defective migration caused by mycolactone. Hence supplementing mycolactone-depleted extracellular matrix may be a future therapeutic avenue, to improve wound healing rates.

Introduction

Buruli ulcer (BU) is a neglected tropical disease caused by subcutaneous infection with *Mycobacterium ulcerans,* characterised by development of large, painless plaques or open lesions, often associated with oedema. The disease is most common in West Africa but is also found in other tropical and subtropical regions including Australia. Although the lesion can be sterilised by a minimum two-month antimicrobial treatment course with rifampicin and clarithromycin, the wounds can take up to a year to heal and can lead to permanent disfigurement, especially when diagnosed late [1]. The polyketide-derived toxin mycolactone, generated by *M. ulcerans*, is the critical driver of BU pathogenesis [2, 3]. Continuous production of this virulence factor causes widespread coagulative necrosis and fibrin deposition in patient skin tissue, as it diffuses through tissue away from the infecting bacteria. Mycolactone is also responsible for the restricted immune response seen in BU. As well as showing long-term cytotoxicity to immune cells [2], mycolactone causes a rapid suppression of antigen presentation, co-stimulation and cytokine secretion at low doses [4, 5].

Many clinical features of BU can be attributed to the inhibitory action of mycolactone on the Sec61 translocon, [6, 7] the complex that translocates most membrane, secretory and organellar polypeptides into the endoplasmic reticulum (ER) [8]. In co-translational translocation, nascent proteins are targeted to the ER surface by a signal peptide sequence at the N-terminus; the interaction between the signal peptide and the pore-forming protein of the translocon, Sec61α, opens a central channel that allows access to the ER lumen and a lateral gate through which transmembrane sequences can enter the membrane [9]. Mycolactone docks to Sec61, preventing signal peptide engagement and locking the translocon in an inactive state with the lateral gate open but the channel blocked [10]. The biogenesis of most secretory proteins and Type I and II membrane proteins is inhibited by mycolactone, while polytopic membrane proteins are largely unaffected [11, 12]. Type III and tail-anchored proteins, which utilise alternative translocation pathways [13], are also resistant

to mycolactone [7, 11, 14]. The proteins whose translocation into the ER is blocked are synthesized in the cytosol where they are degraded by the proteosome [7] and selective autophagy [15, 16]. Sec61 blockade induces an integrated stress response by activation of eIF2α kinases [12, 17] and an increase in autophagic flux [15] and without resolution the cells eventually undergo apoptosis [17, 18]. The time from initial exposure to cell death varies between cell types, but for most human cells takes 3-5 days.

We have previously shown that endothelial cells are particularly sensitive to mycolactone. At low nanomolar concentrations, mycolactone depletes the anticoagulant receptor thrombomodulin [19] and junction proteins [20]. It also increases the permeability of monolayers formed from endothelial cells derived from both vascular and lymphatic origin [20]. While thrombomodulin depletion has also been observed in BU patient skin biopsies [19], this seems not to be the cause of the widespread fibrin deposition commonly seen within the skin tissue. Instead, this is linked to aberrant staining for the extrinsic clotting pathway initiator tissue factor [20]. Tissue factor is normally located in the sub-endothelium where it is segregated from both the plasma proteins that drive coagulation and the surrounding dermal tissue [21]. However, in BU patients, tissue factor was observed within the connective tissue distant from vessels and this spatially associated with fibrin deposition and early signs of necrosis [20]. Our working model leading up to the current work was that mycolactone action at Sec61 in endothelial cells leads to vascular dysfunction and promotes the pathogenesis of BU. The current work seeks to explore the molecular mechanisms driving these events.

The integrity of the endothelium greatly depends on adequate production and maintenance of the extracellular matrix (ECM) [22], junctional complexes [23] and the glycocalyx, a highly charged coating of proteoglycans, glycolipids, glycoproteins and glycosaminoglycans (GAG) including heparan sulphate (HS), chondroitin sulphate (CS) and hyaluronic acid [24] covering the luminal side of the endothelium [25]. The enzymatic glycosylation of heparan and chondroitin sulphate is initiated in the Golgi apparatus by

transferase enzymes. This is also the site of the isomerisation and sulfation reactions needed to achieve the rich diversity of GAGs expressed at the cell surface [26]. The glycocalyx acts as an exclusion zone for blood cells and controls interactions with platelets, blood clotting factors and immune cells as well as modulating fluid exchange and acting as a sensory system for the endothelial monolayer [26]. On the basal side of the endothelium, is the basement membrane (BM), an ECM consisting of collagen type IV and laminins, crosslinked by perlecan, a HS proteoglycan, and/or nidogens [27]. This sheet-like network forms a scaffold that interacts with integrins on the cell surface, controlling structural stability, cell adhesion and angiogenesis as well as preventing leukocyte extravasation [27, 28]. Production of these complex structures, which preserve and regulate the barrier between blood and tissue, relies heavily on Sec61-dependent proteins.

In order to determine the molecular mechanisms driving mycolactone-induced endothelial cell dysfunction we have undertaken a detailed phenotypic and proteomic study of the changes it induces both *in vitro* and *in vivo.* Using primary human dermal microvascular endothelial cells (HDMEC), we found that, as well as increasing monolayer permeability, mycolactone caused rapid changes in endothelial cell morphology and migration, accompanied by loss of glycocalyx, adhesion and ECM proteins. Notably, structurally unrelated Sec61 inhibitors, Ipomoeassin F, and its derivatives induced comparable phenotypes in a similar time frame, highlighting the Sec61 dependency of ECM composition and function. We have dissected the roles of these different components in the response to mycolactone and found that loss of an enzyme critical for GAG biosynthesis phenocopied the changes seen in cell morphology and monolayer permeability. On the other hand, the effects on cell adhesion and migration were dependent on ECM interactions and could be ameliorated by application of exogenous laminin-511. Hence the current work presents a novel pathogenic mechanism in BU, driven by Sec61-dependent effects on endothelial cells.

Results

Sec61 blockade impacts endothelial cell morphology and adhesion

We recently observed that mycolactone induces morphological changes in primary endothelial cells *in vitro*, leading to a dose-dependent increase in monolayer permeability at 24 hours [20]. To understand the longer-term effects of mycolactone, we performed time-lapse imaging of HDMECs exposed to mycolactone (Video 1) or solvent (DMSO) control (Video 2) every 30 minutes for 48 hours. As in previous observations, the cells began to take on an 'elongated' phenotype after 8 hours. The proportion of elongated cells increased with time (Fig 1A) and after 24 hours exposure, approximately half the cells (51.63±2.89%) had this phenotype. The average ratio of cell length to width doubled in 16 hours, and quadrupled after 24 hours exposure (Fig 1C). At 24 hours, a small proportion (9.73±4.01%) had acquired a rounded appearance (Fig 1B) similar to that reported for mycolactone exposure of fibroblasts [16] and epithelial cells [29]. Notably, these cells retained the ability to reattach to the culture vessel (Video 1), in line with their continued viability in this time window [19]. However, after this time their ability to re-adhere declined and the proportion of detached cells steadily increased. Although the number of rounded cells increased between 24 and 48 hours, the elongated phenotype remained predominant at this time point (Fig 1B).

In order to confirm that these phenotypes were relevant to biologically derived mycolactone, we compared the response to the synthetically made mycolactone to that of mycolactone A/B extracted from *M. ulcerans* bacteria. The preparations showed equivalent potency against HDMEC (Figure S1A) and caused similar changes in phenotype in live cell imaging assays (Figure S1B-D).

Next, we investigated how mycolactone affected HDMEC migration using scratch assays. While control cells were successfully able to close the scratch area within 24 hours, mycolactone-exposed cells displayed a gradual cessation in migration into the cell-free gap (Fig 1D). Thus, while at 16 hours similar numbers of cells had migrated into the scratch

regardless of treatment, no further migration could be detected at 24 hours in the presence of mycolactone (Fig 1D). However, it should be noted that mycolactone has previously been reported to cause cell cycle arrest [2], which can be a confounding factor in such migration assays and may explain this finding.

To determine whether Sec61 inhibition by mycolactone was driving these abnormal phenotypes, we exposed endothelial cells to Ipomoeassin F or its more potent derivative, ZIF-80 [30]. These are structurally distinct to mycolactone but inhibit Sec61α in a very similar manner since they compete for the same binding site [31, 32]. Importantly, both compounds phenocopied the 'elongated' appearance preceding detachment in HDMEC within 24 hours (Fig 1E & F). Unbiased analysis of time-lapse data using zenCELL owl built-in algorithms allowed continuous estimation of cell coverage and detachment, although it could not be trained to recognise the elongated phenotype. As expected, cell coverage increased with time under control conditions, while the proportion of detached cells remained constant at approximately 5%. However, all three Sec61 inhibitors showed similar effects on both readouts (Fig 1 G & H), with a similar effect of biologically purified mycolactone (Figure S1E, S1F). Interestingly, both measures remained similar to the control for approximately 24 hours, after which cell coverage declined with a corresponding increase in cell detachment. Taken together, this data strongly supports that these changes are driven by Sec61 inhibition and that endothelial cell homeostasis is dependent on adequate Sec61 function.

As the responses of endothelial cells grown in static culture plates may not accurately reflect *in vivo* behaviour where the cells lining blood vessels are subject to shear stress, HDMEC were cultured on an orbital shaker to more closely mimic conditions experienced under flow. Cells were imaged at the periphery of wells where they experience uniaxial shear stress. Cells were grown to confluency and incubated on a rotary shaker for 24 hours then mycolactone was added. Cell elongation and a uniform alignment of the endothelial cells was maintained for 48hr in the presence of DMSO, as expected (Fig 1I). By contrast, cells exposed to mycolactone became increasingly disorganised over time and by

48 hours a significant proportion were rounded and detached (42.6%, $p<0.05$) (Fig 1I). Although mycolactone did not cause a change in the proportion of elongated cells under these conditions, the pattern of cell rounding was similar to that seen in static cultures (Fig 1J). There was no detectable difference in the length:width ratio at 24 hours, but by 48 hours mycolactone-exposed HDMEC that remained adhered were significantly elongated compared the DMSO control ($p< 0.001$) (Fig 1K). Thus, although the kinetics are slightly different, the phenotypic changes induced by mycolactone in static culture are reproducible in endothelial cells under flow conditions.

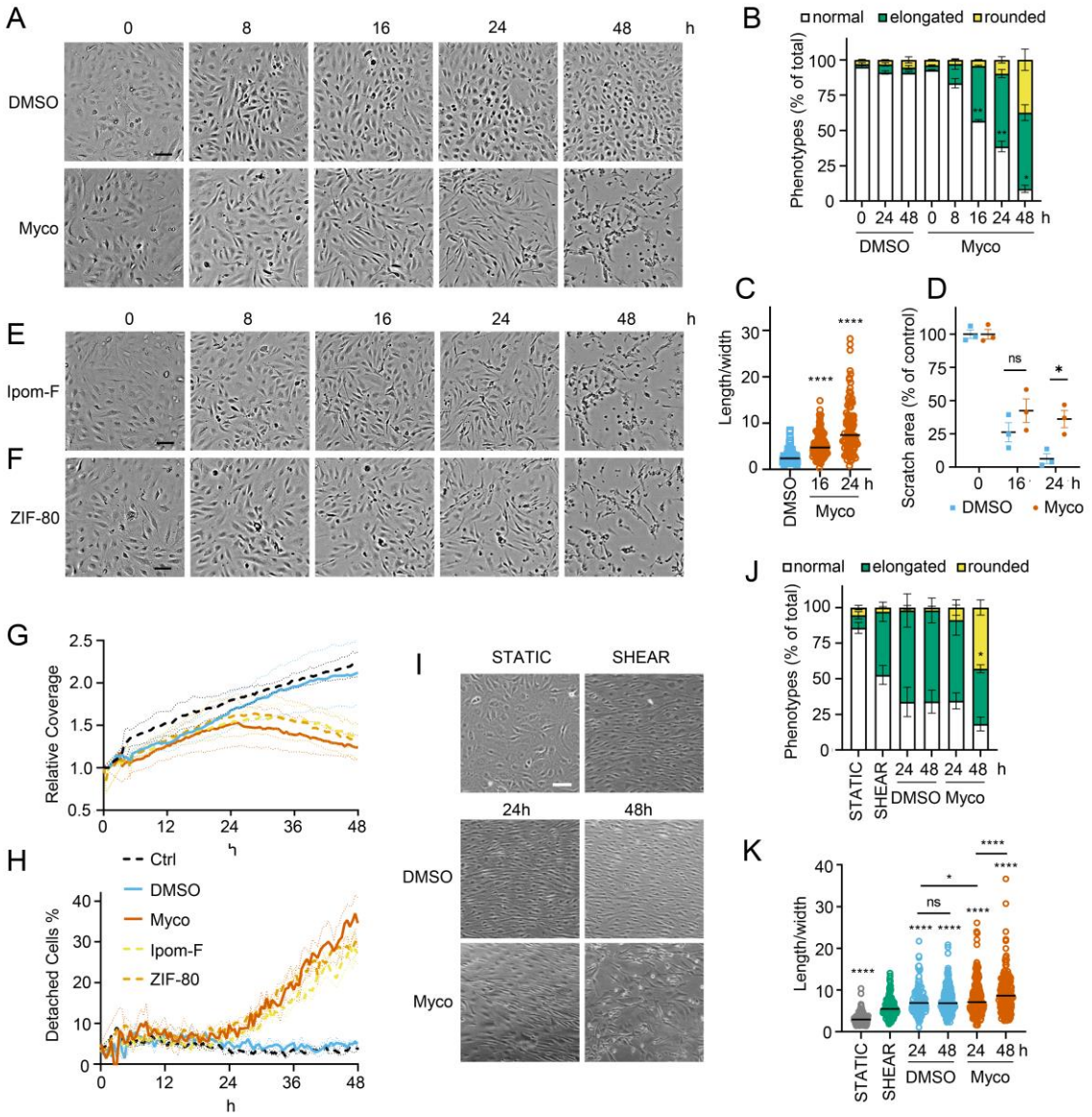

Figure 1. Sec61 inhibition alters endothelial cell morphology and adhesion. HDMECs were exposed to 10 ng/mL mycolactone (Myco), 0.02% DMSO, 400 nM Ipomoeassin F or 20 nM ZIF-80. **A-C**. Mycolactone-treated cells were imaged at indicated times in (**A**) and cell numbers of each phenotype (i.e. normal, elongated or rounded) were counted and presented as a percentage of total cell number per field in (**B**) (mean ± SEM of 3 independent experiments, **, $p<0.01$, *, $p<0.05$. (**C**) Length and width of each cell exposed to mycolactone for 16 and 24 hours or DMSO for 24 hours per image were measured and presented as a ratio. Data is representative of 3 independent experiments. ****, $p<0.0001$ (**D**) A scratch was introduced to a HDMEC monolayer prior to the treatment and visualised at 0, 16, 24 hours. The scratch area is presented as a percentage of the value obtained at 0 hour (mean ± SEM of 3 independent experiments) ns, not significant, *, $p<0.05$. Cells exposed to an alternative Sec61 inhibitor ipomoeassin F (IpomF) (**E**) or ZIF-80 (**F**) were imaged at indicated times. Images are representative of 3 independent experiments. Scale bar = 100 µm. **G-H**. Live cell imaging was performed with the zenCELL Owl incubator microscope every 30 minutes over 48 hours. Algorithms of cell coverage (**G**), detached cell numbers (**H**) per time point from 3 independent experiments are summarised as mean ± SEM. Data presented as cell coverage relative to the value obtained from initial time point (**G**) or a % of detached cells to total cell number (**H**) of each condition. **I.** Confluent HDMECs were incubated on a rotary shaker (SHEAR) or not (STATIC) for 24hr before addition of 0.02% DMSO or 10ng/ml mycolactone and phase-contrast images were taken at 0, 24 and 48hr, within the shear-stress area where appropriate. Data is representative of 3 independent experiments. **J**. Cell numbers of each phenotype at different time points, presented as a percentage of total cell number per field in (**I**), showing mean of 3 independent experiments ± SEM, * $p< 0.05$. **K**. Length and width measurements of cells exposed to mycolactone or DMSO under shear stress conditions for 24 and 48 hours presented as a ratio. Data is representative of 3 independent experiments. ****, $p<0.0001$. Statistical analysis was performed by 2-way ANOVA (panel **B** and **I**) or 1-way ANOVA with Dunnett's (panel **C**) or Tukey's (panel **D**) correction in GraphPad Prism Version 9.4.1. Panel **K** was analysed using a mixed-effects model with Tukey's correction for multiple comparisons.

To establish the *in vivo* relevance of these findings, we performed fibrinogen immunostaining in the pre-ulcerative mouse footpad model of *M. ulcerans* infection (Fig 2, S2). Fibrinogen is a high molecular weight (~330 kDa) plasma protein that is normally retained within the lumen of intact vessels and, indeed, in uninfected (vehicle control) mouse feet, fibrinogen was rarely detected, and then only within the vessel lumen (Fig 2A). In contrast, at 21 days post infection (Grade 1 lesions; metatarsal thickness increase ~10%), fibrin(ogen) was seen within the blood vessel wall surrounding the endothelium (Fig 2B). After 28 days (Grade 2/3 lesions, metatarsal thickness increase 50-100%) widespread fibrin(ogen) staining was seen outside blood vessels within the dermis, in foci consistent with its conversion to insoluble fibrin (Fig 2C). The lack of signal in isotype control-stained tissue (FigS2B) confirms the specificity of staining. This penetration of fibrinogen between the endothelial monolayer lining the vessel, then through the vessel wall and conversion to fibrin by other components of the coagulation cascade within deeper tissue is consistent with our previous findings in human BU patient punch biopsies [20]. Furthermore, the changes in endothelial cell morphology and monolayer integrity described here and previously [20] demonstrates that the extravascular deposition of fibrin is an early feature of infection.

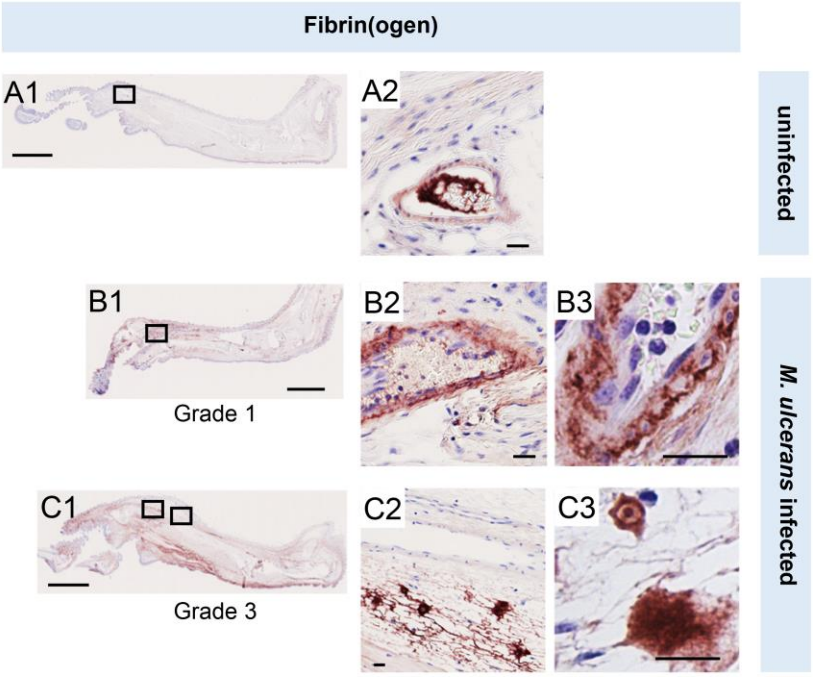

Figure 2. Fibrinogen penetrates the vascular wall at early stages of infection. Immunohistochemistry for fibrin(ogen) in the feet of C57BL/6 mice that received vehicle control (PBS) (A1-2) or intradermal injection of 1 x10^5 colony forming units *M. ulcerans* at 21 (Grade 1; B1-3) or 28 days (Grade 3; C1-3) post-infection. Positive fibrin(ogen) staining is brown in colour, the haematoxylin counterstain is purple. Scale bars in A1, B1 and C1: 2 mm; all others: 20 µm. Data representative of three mice at each infection grade, in two independent infections.

Mycolactone predominantly targets proteins involved in glycosylation and adhesion

While proteomic studies of mycolactone action have been performed previously [6, 12, 14, 16], these have used whole cell lysates, leading to systematic limitations in detection of membrane and secreted proteins, due to their relatively low abundance compared to cytosolic proteins. Therefore, to understand the molecular mechanisms driving the pathogenic phenotypic changes in endothelial cells, we instead used a total membrane proteomics approach to enrich for the Sec61 substrates that are targeted by mycolactone.

We isolated total membrane fractions from HDMECs exposed to DMSO or mycolactone for 24 hours and analysed them by tandem mass tagging (TMT) multiplex LC/MS over biological triplicates (Fig 3A). A total of 6649 proteins were detected, of which 482 were significantly downregulated and 220 upregulated by mycolactone (> 2-Fold

change, $p < 0.05$) (Fig 3B, Supplementary Files 2-5). Among the total proteins discovered, 36.9% were trafficked via the secretory/endolysosomal pathways that primarily depend on the Sec61 translocon (Fig 3C). This group represented 84.6% of the downregulated but only 23.7% of the upregulated proteins. As predicted, membrane proteins were the most affected in the downregulated group, with little effect on cytoplasmic, cytoskeletal, mitochondrial or nuclear proteins. The downregulated fraction included previously published endothelial targets of mycolactone including coagulation regulators thrombomodulin (TM), von Willebrand Factor (vWF), platelet endothelial cell adhesion molecule (CD31), endothelial protein C receptor and tissue factor pathway inhibitor (TFPI) and cell junction components tyrosine protein kinase receptor TIE1, angiopoietin-1 receptor (TEK), cadherin 5 (CDH5), junctional adhesion molecule 3 (JAM-3) and catenin β1 [19, 20] (Fig S3A), validating our dataset.

As seen in previous proteomic studies and *in vitro* translocation assays [11, 12, 33, 34], mycolactone preferentially targeted secreted and single pass type I and type II membrane proteins in endothelial cells, with no effect on the EMC-dependent Type III proteins or the GET pathway-dependent tail-anchored proteins (Fig 3D). A small number (51 out of 606 detected) of multi-pass membrane proteins were also >2-fold downregulated by mycolactone (Supplementary File 6). This group was relatively enriched for signal peptide-bearing proteins (42% vs 4% amongst unchanged and upregulated multi-pass proteins) (Fig 3E). The rules governing sensitivity of this subgroup to mycolactone appear to be similar to those reported for single pass type I proteins [12], with higher signal peptide hydrophobicity and a shorter distance between the signal peptide and first transmembrane domain being associated with increased resistance to the effects of mycolactone (Fig S3B and C). Of the remaining mycolactone-sensitive multi-pass proteins, 80% contained at least one long loop (>50aa) between transmembrane domains. Among the upregulated proteins, 88% of the integral membrane proteins were multi-pass membrane proteins, and only one of the

predicted single pass proteins contained a signal peptide. Likewise, the four upregulated secreted proteins identified are all secreted by non-conventional pathways.

Overall, the data support the recently described model for the biogenesis of multi-pass proteins whereby the majority of multimembrane spanning proteins utilise an alternative translocon that includes Sec61 and the PAT, GEL and BOS complexes but, crucially, bypasses the lateral gate, instead relying on generation of a lipid-filled cavity on the opposite side of Sec61 [35, 36]. Here, only those multi-pass proteins possessing a signal peptide or long internal loops require insertion into the membrane via the Sec61 channel, and therefore only these are sensitive to mycolactone.

Our membrane targeted approach identified a higher number of Sec61-dependent proteins in our control cells compared to previous studies [6, 12, 14] thus achieving our goal of wider capture of mycolactone-sensitive proteins. Moreover, when compared to siRNA-based Sec61α knockdown in Hela cells, despite the differences in cell type and methodology, 100 of the downregulated proteins were common to both datasets (Fig 3F) [37]. While possession of a signal peptide or anchor appears to be crucial to mycolactone sensitivity [12], overall, no specific signal peptide sequence features were associated with downregulation. In keeping with this, there was very little overlap between mycolactone downregulated proteins and those lost following knockdown of translocon-associated proteins TRAPβ or knockout of Sec62/Sec63 (Fig S3D and S3E) [37, 38], which assist gating of the translocon by weak signal peptides. Thus, as suggested by analysis of the structure of the inhibited translocon [10], mycolactone acts via direct interaction with the Sec61α signal peptide binding site rather than through interference with accessory proteins.

Gene ontology (GO) analysis of mycolactone-upregulated proteins supported previous observations by ourselves and others of cellular stress responses, with significant enrichment of terms associated with oxidative stress and detoxification (Fig 3G) [12, 17, 39, 40]. The upregulated proteins also included several proteins involved in the autophagy pathway, including SQSTM1/p62, which is involved in the cellular response to mycolactone

[15] (Fig S3A). However, in the significantly downregulated fraction a distinct pattern emerged, with GO terms associated with glycosylation, matrix organisation, adhesion and cell migration showing the greatest over-representation compared to the whole genome. Within these GO groups, the vast majority of proteins detected in our proteome were downregulated by mycolactone (Fig 3H). Similar results were obtained when the downregulated proteins were compared to the total detected proteome (Fig S3F), showing this pattern was not an artefact resulting from membrane enrichment.

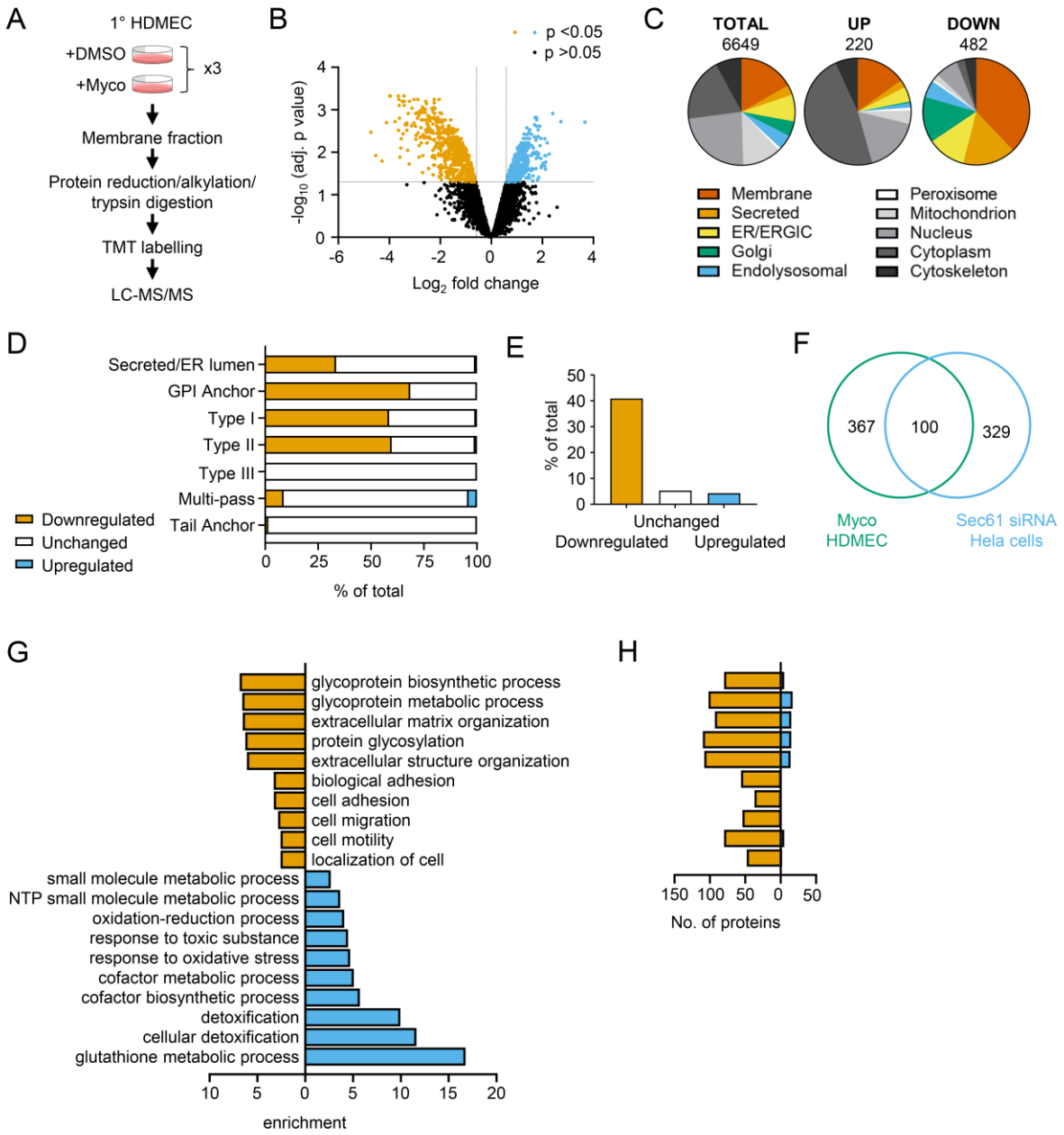

Figure 3. Proteomic analysis reveals loss of proteins associated with glycosylation, adhesion and migration. (**A**) Workflow for isolation and proteomic analysis of HDMEC membrane proteins. In 3 independent replicates, HDMEC were exposed to 10ng/ml mycolactone or DMSO for 24 hours, lysed by hypotonic lysis and membrane fractions enriched by differential centrifugation as described in Methods. Acetone precipitated proteins were reduced, alkylated and trypsinised then subjected to TMT labelling for quantitative proteomic analysis by LC-MS/MS. (**B**) Volcano Plot of differential expression between DMSO and mycolactone treated samples, plotting mean fold change against false discovery rate adjusted *p*-values; orange= downregulated, $p<0.05$; blue= upregulated, $p<0.05$; black=p>0.05 (**C**) Pie charts showing subcellular localisation of proteins in total, >2 fold upregulated or downregulated ($p<0.05$) fractions. (**D**) Quantitation of membrane or secreted proteins according to type: blue = upregulated; white = unchanged; orange = downregulated. (**E**) Percentage of downregulated, unchanged and upregulated multi-pass membrane proteins possessing a signal peptide. (**F**) Overlap between mycolactone downregulated endothelial membrane proteome and Sec61-dependent proteome. Venn diagram created using JVenn [41], showing overlap in significantly downregulated proteome between the dataset presented here and those obtained in Hela cells treated with siRNA for Sec61α (Nguyen et al., 2018). (**G**) Top significantly over-represented ($p<0.05$) GO groups in downregulated and upregulated data sets, compared to whole genome. Data generated with WebGestalt. (**H**) Quantitation of numbers of up and down regulated proteins in GO groups identified in (**G**).

Mycolactone disproportionately targets Golgi-resident proteins involved in glycosylation and glycosaminoglycan chain synthesis leading to the loss of surface GAGs

The Golgi is the site of higher order protein glycosylation and GAG synthesis and, of the intracellular organelles, is the most affected by mycolactone (Fig 3C and S4A). The Golgi has a particularly high proportion of type II membrane proteins as the membrane anchor and sequences around it can act as a signal for Golgi retention [42] and nearly all of these Golgi-expressed type II membrane proteins were significantly downregulated by mycolactone (Fig 4A). Interestingly, type II Golgi proteins showed a higher degree of down-regulation by mycolactone than ER or plasma membrane localised type II proteins (Fig 4B). This suggests the signals that lead to Golgi localisation may make proteins more sensitive to Sec61 inhibition, although it is equally possible that Golgi proteins are turned over at a higher rate than those at other sites as depletion is generally at the turnover rate [19]. The effect is not due to differences in transmembrane domain hydrophobicity, which shows little variation and has no impact on Type II protein levels in mycolactone-treated cells (Fig S4B).

Detailed analysis of our dataset revealed that targeting of Golgi-localised proteins by mycolactone leads to significantly decreased abundance of multiple enzymes involved in both higher order N- and O-linked glycosylation (Fig 4C). However, the biggest impact is seen in GAG production, with the majority of the enzymes involved in GAG synthesis lost in mycolactone treated HDMECs (Fig 4D and S4C). All of the 23 proteins in the GAG biosynthetic pathway detected in our analysis are type II membrane proteins and 19 (82%) of these were downregulated by mycolactone (Fig 4D), affecting every step of glycosaminoglycan production (Fig S4C). Three of the mycolactone-targeted proteins were involved in initial steps of keratan sulphate formation, four in common synthesis initiation of chondroitin sulphate (CS), dermatan sulphate (DS) and heparan sulphate (HS), six in chain elongation of CS/DS and HS (two and four, respectively), and six in epimerisation or sulfation processes that enhance the structural diversity of CS/DS or HS (Fig 4D and S4C).

Given the importance of GAGs to endothelial function and the dramatic loss in GAG biosynthetic enzymes induced by mycolactone, we evaluated surface levels of the predominant endothelial GAGs, HS, and CS, using flow cytometry on HDMECs exposed to mycolactone for 24 hours. As a control, chondrointinase ABC was used to remove surface CS, resulting in fluorescence levels 60% lower than untreated cells. Remarkably, CS fluorescence intensity was even lower in cells exposed to mycolactone (Fig 4E). Similarly, using an antibody specific for a neoepitope of HS generated by heparinase III digestion, dHS, disrupted surface HS expression was observed in mycolactone-exposed cells (14.11±7.40% vs. DMSO solvent control 105.30±9.79%, $p = 0.0002$, Fig 4F). In addition, HS-containing proteoglycans were detected by immunoblot using the anti-dHS antibody. Heparinase III digestion revealed an abundance and diversity of heparan sulphate containing proteins present in untreated or DMSO-exposed HDMECs that decreased progressively with mycolactone exposure (Fig 4G). By immunofluorescence, HS forms a mesh-like network around and between cells in untreated and DMSO solvent controls (Fig 4H). However, in HDMECs exposed to mycolactone, or ZIF-80, the HS-positive network was disrupted within 20 hours (Fig 4H). Collectively, this data confirms that Sec61 inhibition by mycolactone profoundly impairs the ability of endothelial cells to synthesise GAG chains.

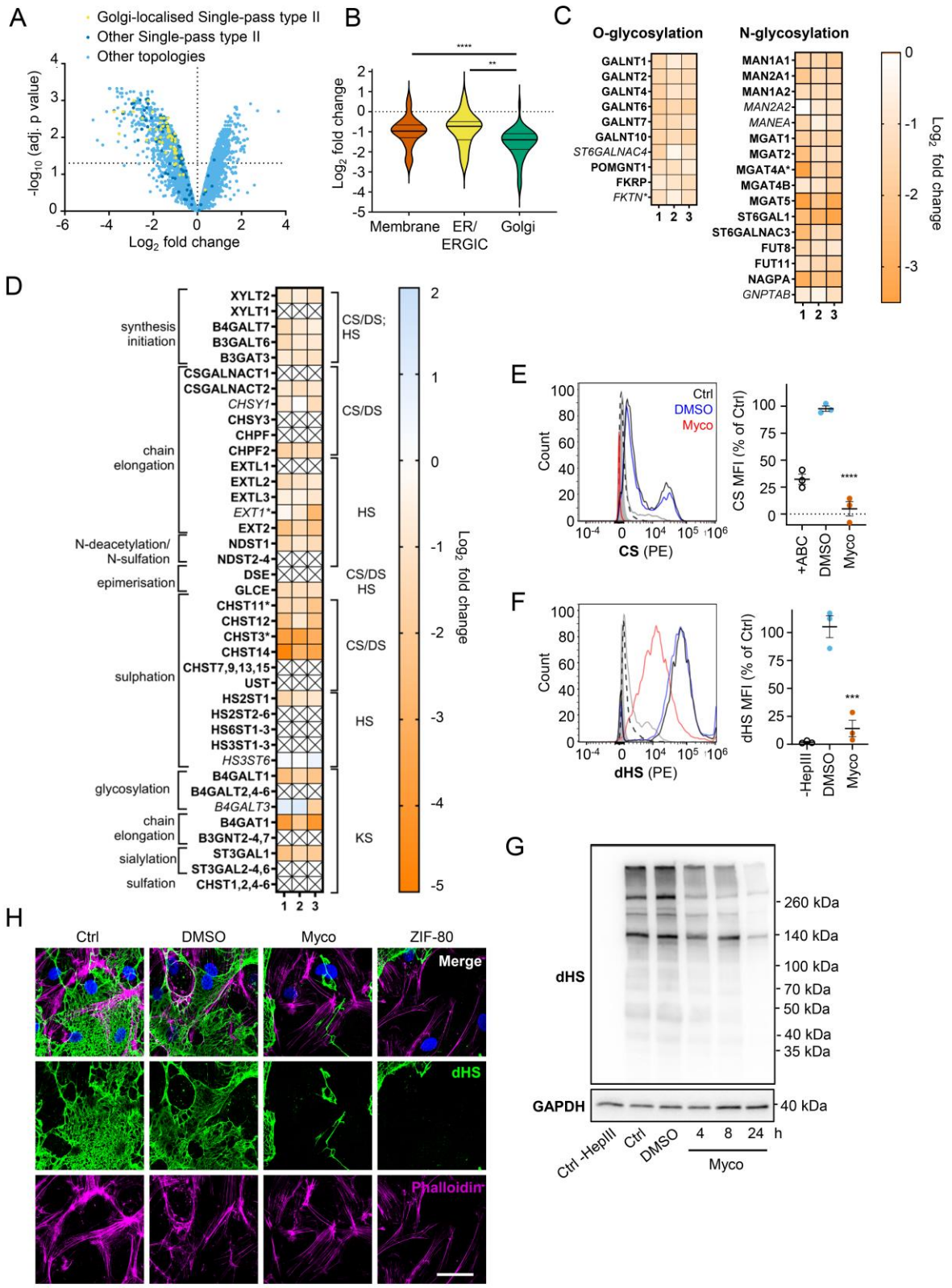

Figure 4. Endothelial glycosaminoglycan chain synthesis is blocked by mycolactone. HDMECs exposed to 10 ng/mL of mycolactone (Myco) or 0.02% DMSO for 24 hours or indicated times were subjected to proteomic analysis (**A-D**), surface immunostaining (**E-F, H**) or immunoblotting (**G**). (**A**) Volcano Plot of differential expression between DMSO and mycolactone treated samples, plotting mean fold change against false discovery rate adjusted *p*-values. Pale blue=total detected proteins; dark blue=Type II membrane proteins; yellow=Golgi-localised Type II membrane proteins. (**B**) Violin plot showing fold change in protein levels for Type II membrane proteins grouped according to subcellular location. ns, not significant; **, $p < 0.01$; ****, $p < 0.0001$. (**C**) Heat map

showing fold change in Golgi-localised O- and N-glycosylation enzymes in mycolactone exposed HDMEC. Dual-colour coding is shown., only one unique peptide detected in asterisks, and significantly downregulated ($p < 0.05$) or not ($p \geq 0.05$) in bold or *Italic* respectively. (**D**) Genes in GAG biosynthesis categorised according to function and side chains of chondroitin sulphate/ dermatan sulphate (CS/DS), heparan sulphate (HS) or keratan sulphate (KS). Heatmap showing Log2 fold change of these genes in response to mycolactone in three independent experiments. Dual-colour coding is shown. Genes undetected are indicated as crossed, only one unique peptide detected in asterisks, and significantly downregulated ($p < 0.05$) or not ($p \geq 0.05$) in bold or *Italic* respectively. (**E-F**) Cells were treated with or without chondroitinase ABC (ABC) or heparinase III (HepIII), immunostained with anti-chondroitin sulphate (CS), anti-Δ-heparan sulphate (dHS) antibodies or the isotype controls for flow cytometry analysis. Histogram plot for single cell population of CS (E) and dHS (F) and the respective mean fluorescence intensity (MFI) are shown. Unstained untreated cells filled grey; isotype control of untreated cells, dashed line in black; Untreated cells incubated with chondroitinase ABC prior to CS staining or without HepIII prior to dHS staining, grey line; untreated cells with CS-PE or dHS-PE, black line; cells exposed to DMSO stained with antibodies, blue line; cells exposed to mycolactone stained with antibodies, red line. MFI is presented as a % of untreated control (mean ± SEM of 3 independent experiments). **, $P < 0.01$; ***, $P < 0.001$; ****, $P < 0.0001$. (**G**) Cells were lysed, treated with heparinase III and analysed by immunoblotting. HS neoepitopes were visualised with anti- Δ-heparan sulphate (dHS) antibody with the approximate migration of molecular weight markers in kDa. GAPDH as loading control. Images are representative of 3 independent experiments. (**H**) Cells were incubated with HepIII, fixed and immunostained with anti-dHS antibody (green), permeabilised and labelled with TRITC-conjugated phalloidin (magenta). Nuclei were stained with DAPI (blue). Images are representative of 2 independent experiments. Scale bar = 50 µm. Statistical analysis was performed 1-way ANOVA with Tukey's (panel **B**) or Dunnett's (panel **E**&**F**) correction for multiple comparisons in GraphPad Prism Version 9.4.1.

Loss of galactosyltransferase II drives changes in endothelial cell morphology and monolayer permeability

We reasoned that mycolactone-dependant depletion of any enzyme involved in the early stages of GAG biosynthesis would, on its own, be sufficient to explain the loss of HS and CS. Therefore, we validated its effect on the GAG linker building enzyme galactosyltransferase II (B3GALT6) by immunofluorescence. Endothelial B3GALT6 colocalised with the Golgi marker GOLGB1/Giantin in a perinuclear region in untreated cells and was unchanged in those exposed to the solvent control (0.02% DMSO) (Fig 5A). B3GALT6 expression levels remained normal in HDMECs exposed to mycolactone for 6 hours but a clear reduction was seen after 12 hours (Fig 5A). Similar findings were made with biological mycolactone (Figure S5A). Notably, ZIF-80 reduced B3GALT6 expression in a similar manner (Fig S5B).

In order to investigate whether loss of B3GALT6 was sufficient to induce the phenotypic changes we saw after mycolactone exposure, we knocked down B3GALT6 in HUVECs using siRNA. The reduction in B3GALT6 protein expression compared to cells transfected with non-targeting si-control RNA (Fig 5B) was comparable to that caused by mycolactone (~80%). B3GALT6 siRNA-treated cells demonstrated a similar elongated appearance (Fig 5C) and image analysis confirmed a significant increase in the ratio of cell length to width in HUVECs transfected with si-B3GALT6 RNA (Fig 5D). However, knockdown of B3GALT6 did not recapitulate the cell rounding phenotype (Fig 5E).

We next investigated the potential contribution of B3GALT6 loss to the previously observed mycolactone-induced increase in HDMEC and human dermal lymphatic endothelial cell monolayer permeability [20]. Exposure of mock-transfected HUVEC monolayers to 10 ng/mL mycolactone for 24 hours increased permeability to 23.13±7.38%, an effect comparable to 100 ng/mL IL-1β (21.30±3.48%) (Fig 5E). B3GALT6 knockdown in HUVECs also led to a rise in monolayer permeability (10.08±4.37% and 15.47±1.27% of the values seen in empty wells, $p = 0.2371$ and 0.0367, for two different oligonucleotides, Fig 5F). Interestingly, B3GALT6 knockdown did not reduce the rate of HUVEC migration in scratch assays (Fig 5G); instead the cells exhibited a slightly increased healing rate compared to controls.

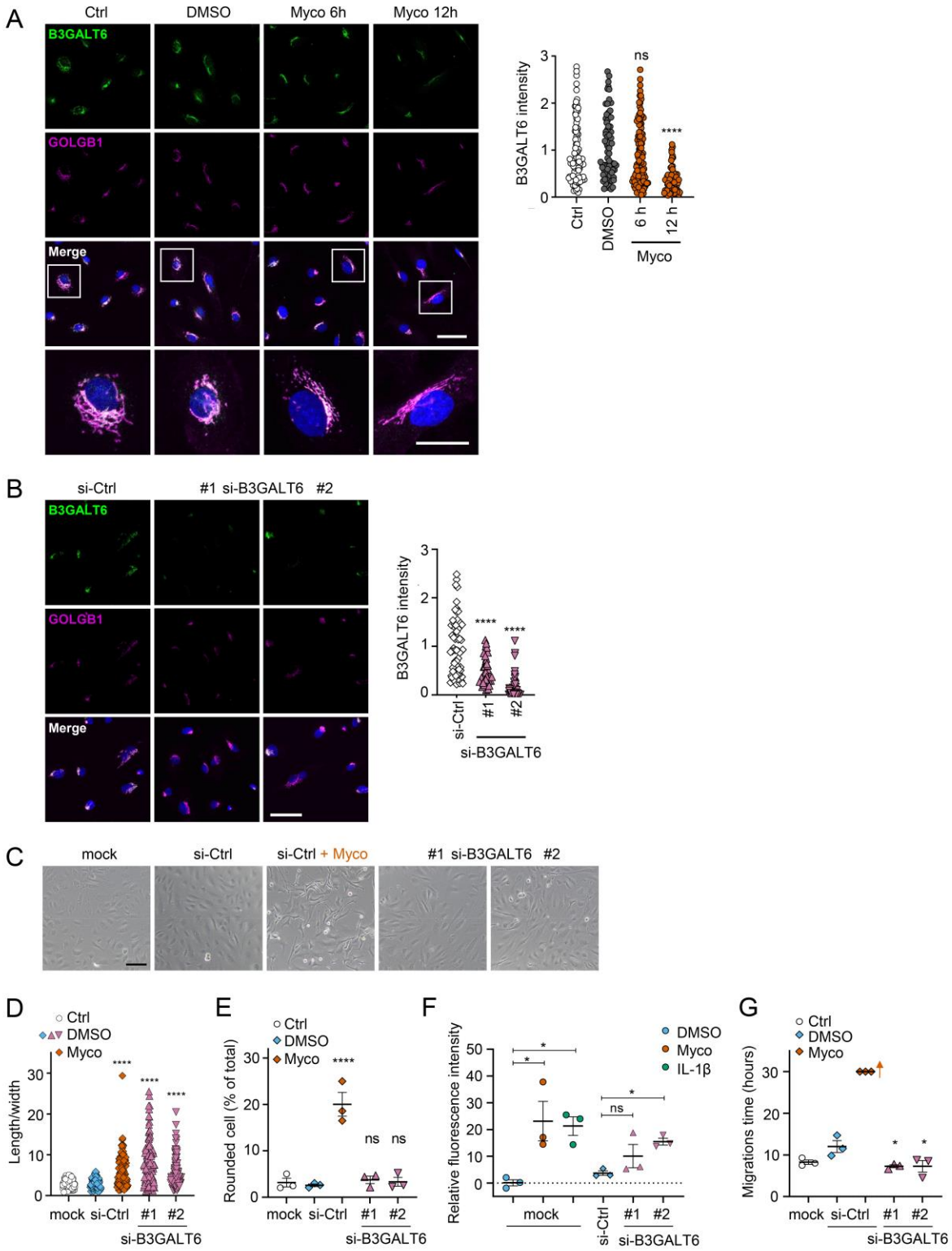

Figure 5. Loss of B3GALT6 affects endothelial cell morphology and monolayer permeability. A. HDMECs exposed to 10 ng/mL mycolactone (Myco) or 0.02% DMSO for indicated times. **B-G**. HUVECs transfected with si-B3GALT6 or si-negative control (ctrl) oligos for 48 hours. (**A-B**) Cells were fixed, permeabilised and immunostained with anti-B3GALT6 and anti-GOLGB1 antibodies. B3GALT6 (green) and the Golgi apparatus (magenta) were visualised and nuclei stained with DAPI (blue). Scale bar = 50 µm (20 µm in the crop panels of **A**). Corrected total cell fluorescence of B3GALT6 in Golgi apparatus per cell was measured and presented as a value normalised to the mean value obtained from untreated control of each experiment. More than 30 cells per condition were measured per experiment. Images and quantification are representative of 3 independent

experiments. (**C-E**) HUVECS exposed to 10 ng/mL mycolactone (Myco) or 0.02% DMSO for 24 hours one day post-transfection were imaged by an inverted microscope. (**D**) Length and width of each cell presented as a ratio. At least 100 cells were measured for each treatment. Values are representative of 3 independent experiments. (**E**) Rounded cell number per image presented as a % of total cell number per condition (values represent the mean ± SEM of 3 independent experiments). (**F**) Permeability of transfected HUVEC monolayers on inserts with 1 µm pores treated with 100 ng/mL IL-1β, 10 ng/mL mycolactone (Myco) or 0.02% DMSO for 24 hours was quantified. Fluorescence intensity of FITC-dextran in the receiver wells was measured and presented as a % where 100% is the value obtained from transwell lacking a cell monolayer, and 0% is untreated control wells (mean ± SEM of 3 independent experiments). (**G**) HUVECs were transfected with si-B3GALT6 or si-negative control (si-ctrl) oligos. A scratch was introduced to the monolayer prior to the treatment (10 ng/mL mycolactone (Myco) or DMSO) and live cell imaging was performed with the zenCELL Owl incubator microscope every 15 minutes for 30 hours. Migration time in hours (hrs) to reform the monolayer is presented as mean ± SEM (n = 3); wells with no visible monolayer at the end point were given a maximum value = 30. ns, not significant; *, $P < 0.05$; ****, $P < 0.0001$. Statistical analysis was performed using 1-way ANOVA with Dunnett's correction for multiple comparisons in GraphPad Prism Version 9.4.1 (all analysed panels).

Mycolactone rapidly depletes endothelial surface proteoglycans

Since loss of GAGs did not explain all the phenotypes observed, we considered the so-called core proteins to which GAGs synthesised in the Golgi are covalently linked to form the proteoglycans. These can be secretory, plasma membrane or GPI-anchored proteins, all of which require the Sec61 translocon for their biogenesis. Our proteome revealed that seven HS, CS, and/or DS-carrying proteoglycans were significantly down-regulated after 24 hours mycolactone exposure (Fig 6A).

Using flow cytometry, we validated the changes in abundance of three cell surface proteoglycans; perlecan (HSPG2; secreted, HS/CS), glypican-1 (GPC1; GPI-anchored, HS/CS) and biglycan (BGN; secreted, CS/DS). Syndecan-2, a membrane-bound protein for which only one unique peptide was found in the proteome, could not be detected by flow cytometry. The most profound effects were seen for perlecan and glypican-1 (detection at 10.8±4.8% and 28.8±9.0% of untreated control, Fig 6B), while biglycan was partly reduced (43.7±6.8% of untreated control). As the turnover rate of HS proteoglycans is rapid ($t_{1/2}$= 3-4 hours in granulosa and 6.9 hours in macrophages [43, 44]), we explored the rate of perlecan and glypican-1 loss at early time points in HUVECs. A ~50% reduction in perlecan was

evident after only 2 hours mycolactone treatment, reaching significance at 6 hours. Depletion of glypican-1 was slower, evident at 6 hours and reaching significance at 24 hours (Fig S6A).

Immunofluorescence staining of HDMECs showed abundant perlecan staining in control cells, particularly around intercellular junctions, but the staining rapidly decreased in response to mycolactone, with reduced expression detectable after 8 hours (Fig 5C). HDMECs exposed to ZIF-80 for 8 hours displayed similarly limited perlecan-positive junctional staining (Fig 6C), and the depletion was duplicated when biological purified mycolactone was compared to synthetic material (Fig S6B), and also occurred when the endothelial cells were under shear stress (Fig S6C). The parallel loss of GAGs and the proteoglycans that bear them means that the glycocalyx is severely disrupted by mycolactone.

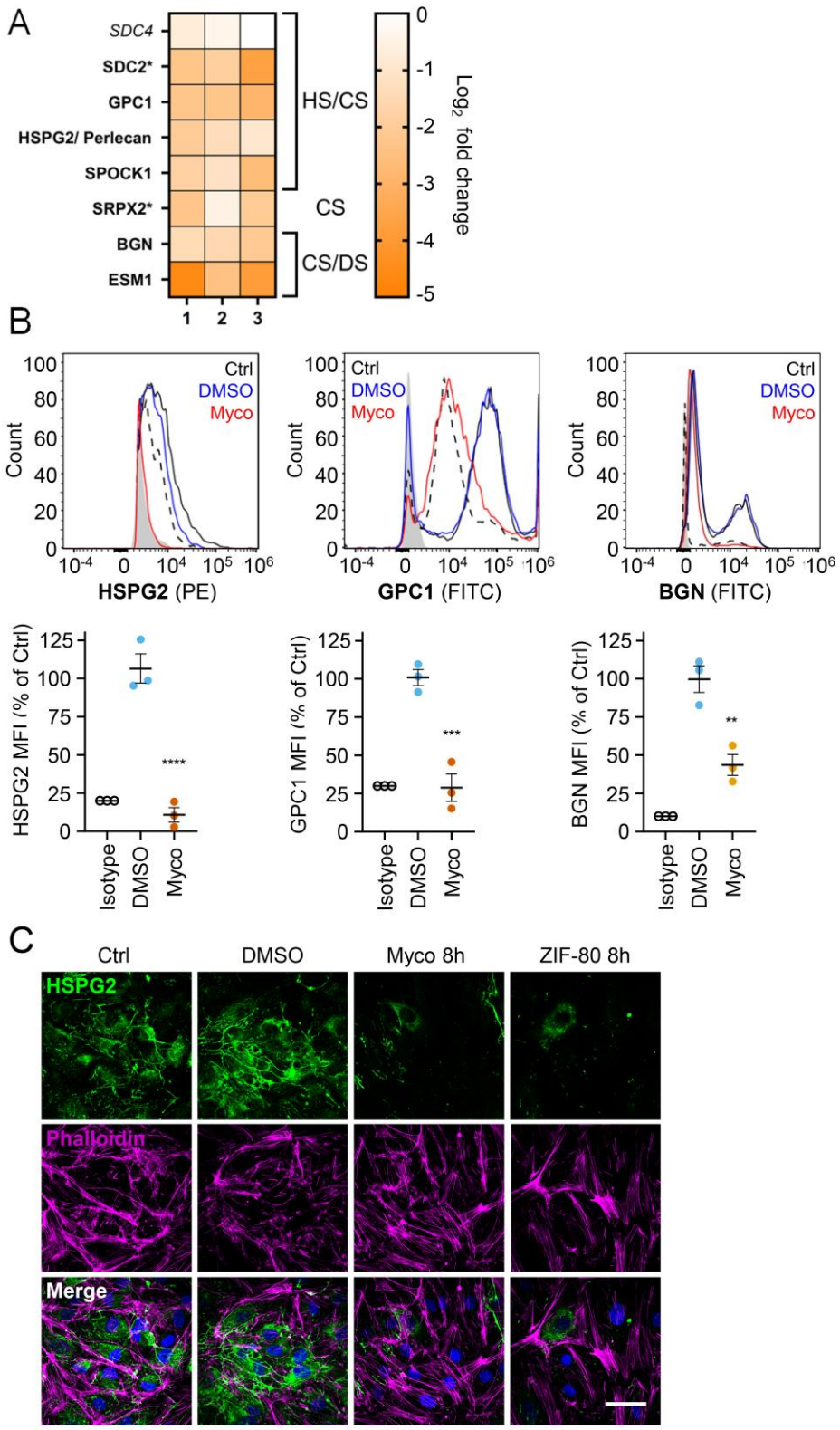

Figure 6. Mycolactone causes a rapid loss of multiple proteoglycans. HDMECs exposed to 10 ng/mL mycolactone (Myco), 0.02% DMSO or 20 nM ZIF-80 for 24 hours or indicated times. (**A**) Heatmap showing representative data for genes encoding proteoglycans. Dual-colour coding for log2 fold change in response to Myco is shown. Possible attached glycosaminoglycan chains such as heparan sulphate (HS), chondroitin sulphate (CS) or dermatan sulphate (DS) Candidates with one unique peptide detected indicated with asterisks, significantly downregulated ($p < 0.05$) or not ($p \geq 0.05$) in bold or *Italic* respectively. (**B**) Cells were harvested for flow cytometry analysis. Histogram plots for single cell population of perlecan, glypican-1 and biglycan. Unstained untreated cells, filled grey; isotype control of untreated cells, dashed black line. untreated cells stained with

antibodies, black line; cells exposed to DMSO stained with antibodies, blue line; cells exposed to MYC stained with antibodies, red line. MFI is presented as a % of untreated control (mean ± SEM of 3 independent experiments). **, $P < 0.01$; ***, $P < 0.001$; ****, $P < 0.0001$. (**C**) Cells were fixed and immunostained with anti-perlecan antibody (green), permeabilised and labelled with TRITC-conjugated phalloidin (magenta). Nuclei were stained with DAPI (blue). Images are representative of 3 independent experiments. Scale bar = 50 µm. Statistical analysis was performed using 1-way ANOVA with Dunnett's correction for multiple comparisons in GraphPad Prism Version 9.4.1 (all analysed panels).

Mycolactone depletes endothelial basement membrane components and their ligands

Taken together, our results so far show that mycolactone profoundly depletes the endothelial glycocalyx, due to the loss of both GAG and proteoglycan biosynthesis following Sec61 inhibition. However, while loss of GAG production affected permeability, it had less impact on adhesion and migration. We therefore next focused on the downregulated proteins in our dataset with GO classifications linked to these processes. Numerous adhesion molecules and basement membrane components were downregulated by mycolactone, including nidogen 1 (NID1), laminins and collagens (Fig 7A). Although the abundance of major BM component collagen IV was not significantly influenced by mycolactone, perhaps indicating a slow turnover rate, several ER-localised and/or secreted enzymes involved in collagen biosynthesis (Table S3), were reduced as previously reported in murine fibroblasts [16]. Laminins are the other key constituent glycoproteins of the BM and important binding partners for endothelial cell integrins. Our proteomic data suggested multiple laminins are affected by mycolactone. Laminin α4 and α5 are both common to all types of vessel wall, but α4 has a slightly higher turnover rate [45]. By immunofluorescence staining, laminin α4 was seen in perinuclear regions within cells and in the network bridging intercellular junctions between endothelial cells in untreated and DMSO control HDMEC (Fig 7B). After 16 hours of exposure to mycolactone, the perinuclear staining was absent and the laminin-positive network between cells had become disconnected (Fig 7B). Similar findings were made in biological purified mycolactone was compared to synthetic material (Fig S7A). Loss of laminin α4 staining was also observed in endothelial cells exposed to mycolactone

under shear stress (Fig S7B). The same striking decrease was also seen in HDMECs exposed to ZIF-80 (Fig 7B).

The effect of mycolactone on the abundance of the laminin binding integrin β subunits β1 and β4 and laminin α5 in HDMEC were determined by flow cytometry (Fig 7C). After 24 hours, they were reduced to 45.0±6.2%, 27.3±7.7% and 15.6±5.4% respectively of control levels (Fig 7C). In addition, the loss of expression of the basement membrane component fibronectin and cell surface integrin α5 were validated using immunoblot analysis; fibronectin levels decreased very rapidly showing >75% depletion after 4 hours exposure to mycolactone ($p<0.01$) (Fig S7A) whilst the level of integrin α5 decreased more slowly, reaching ~50% of control levels at 24h ($p<0.01$; Fig S7B).

To determine whether the basement membrane was disrupted *in vivo*, we stained the tissue sections from *M. ulcerans*-infected mice with the alcian blue-periodic acid Schiff (AB-PAS) method. In mouse feet receiving the vehicle control (Fig 7D1), the dermis contained neutral glycans (purple staining) and the vasculature displayed an intact vessel basement membrane (Fig 7D4, insert). At early stages of infection (Grade 1; Fig 7D2), immune cell infiltration could be seen in these regions in proximity to mycobacterial clusters (Fig S2A) and the surrounding dermal tissue had become more acidic (blue staining) (Fig 7D5). At later stages of infection, when the metatarsal area was more swollen (Fig 7D3) and the dermis showed marked oedema and the fibrous architecture was disrupted (Fig 7D6-7), there was an overall reduction in the intensity of staining around the vasculature and the vessel basement membranes were irregular (Fig 7D6, insert).

To confirm the impact of infection on the basement membrane we used transmission electron microscopy (Fig 7E) to characterize the early vascular changes in the podal dermis of mice inoculated with *M. ulcerans*. Multiple transverse, oblique and longitudinal sections of arterioles, venules and lymphatics were examined. In Grade 1, the interstitium surrounding the capillary was expanded by electron-lucent granular material, pericyte processes were

often separated and collagen fibrils close to the blood vessels increasingly disaggregated. The endothelial cells exhibited varying degrees of swelling and vacuolation with an irregular luminal surface including cytoplasmic undulation and projections. The subendothelial basement membrane appeared multifocally disrupted, expanded or discontinuous (Fig 7E, arrows). Taken together the data shows that even at early stages of infection, the endothelial basement membrane is compromised and the loss of constituent proteins caused by mycolactone is likely a major factor in these changes.

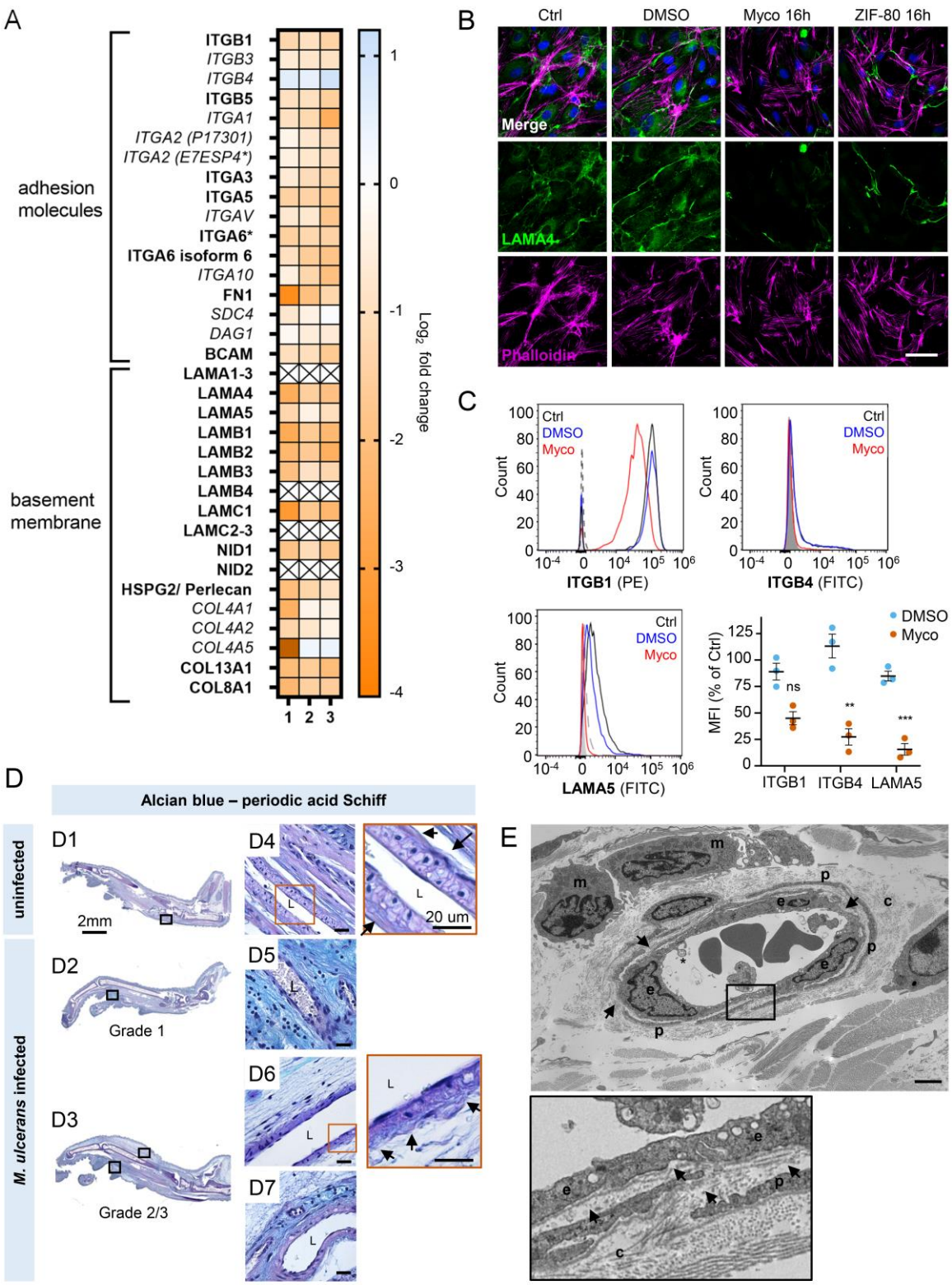

Figure 7. Mycolactone interferes with the interaction between endothelial surface receptors and the basement membrane. HDMECs exposed to 10 ng/mL mycolactone (Myco), 0.02% DMSO or 20 nM ZIF-80 for 24 hours or indicated times. (**A**) Heatmap showing representative data for genes encoding junctional or adhesion molecules, basement membrane components and proteins involved in platelet adhesion. Dual-colour coding for log2 fold change in response to Myco is shown. Candidate with one unique peptide detected is indicated with asterisks, significantly downregulated ($p < 0.05$) or not ($p \geq 0.05$) in bold or *Italic* respectively. (**B**) Cells were fixed and immunostained with anti-laminin α4 antibody (green), permeabilised and labelled with TRITC-conjugated phalloidin (magenta). Nuclei were stained with DAPI (blue). Images are representative of 2 independent

experiments. Scale bar = 50 µm. (**C**) Cells were harvested for flow cytometry analysis. Histogram plots for single cell population of integrin β1, integrin β4 and laminin α5. Unstained, untreated cells, filled grey; isotype control of untreated cells, dashed black line. untreated cells stained with antibodies, black line; cells exposed to DMSO stained with antibodies, blue line; cells exposed to Myco stained with antibodies, red line. MFI is presented as a % of untreated control (mean ± SEM of 3 independent experiments). ns, not significant; **, $P < 0.01$; ***, $P < 0.001$; ****, $P < 0.0001$. (**D**) Alcian blue-periodic acid Schiff stain in the feet of C57BL/6 mice that received vehicle control (PBS) (D1, D4) or intradermal injection of $1*10^5$ colony forming units *M. ulcerans* at 21 (Grade 1; D2, D5) or 28 days (Grade 2/3;I3, D3, D6-7) post-infection**.** Neutral glycans are indicated by purple staining and acidic glycans by light blue Blood vessel lumens are indicated by an "L". Scale bars in D1-3: 2 mm; all others: 20 µm. **E** Representative transmission electron microscopy scan of grade 1 *M. ulcerans* infected murine footpad. The ultrathin section of glabrous skin shows the pericapillary interstitium slightly expanded, collagen (c) fibrils variably disaggregated and infiltrating macrophages (m). The endothelial cells (e) are reactive and exhibit cytoplasmic projections (*) whilst the basement membrane is multifocally disrupted (arrows). A thin layer of pericytes (p) is variably expanded by oedema. Scale bar: 2µm. Statistical analysis was performed using 1-way ANOVA with Dunnett's correction for multiple comparisons in GraphPad Prism Version 9.4.1 (Panel **C**).

Exogenous laminin-α5 ameliorates mycolactone-driven cell detachment and impaired migration

Since laminins are secreted proteins, which are then deposited to form cell-associated extracellular matrix, we wondered whether exogenous provision of these molecules might protect mycolactone-exposed cells. We therefore coated tissue culture plates with laminin-111, -411 or -511, complexes that contain laminin β1γ1 in combination with laminins α1, α4 or α5 respectively. As expected [46], primary HDMECs efficiently re-attached to laminin-511-coated culture vessels, with very little reattachment to uncoated vessels ($p = 0.0020$, Fig S8A). Re-attachment laminin-411 or the non-endothelial specific laminin-111 was also observed albeit to a lesser extent ($p = 0.1226$ and 0.3365 compared to the uncoated wells, respectively). We then quantified the re-attachment of endothelial cells that had been pre-exposed to mycolactone for 24 hours compared to controls (Fig 8A). Remarkably, mycolactone-exposed cells re-adhered to specifically to laminin-511- (but not 411- or 111-) coated vessels with the same efficiency as controls (Fig 8A).

We then investigated whether exogenous laminin-511 could ameliorate the cell rounding, attachment or migration phenotypes observed in response to mycolactone using time-lapse imaging of HDMECs. On uncoated wells, mycolactone caused the expected

phenotypic changes (Fig 8B-C), and remarkably, exogenous laminin α5 significantly reduced mycolactone-driven cell rounding, even after 48 hours (7.7±1.5% vs. 17.6±2.4%, $p = 0.0194$, Fig 8B). Similarly, while the relative number of attached cells did not increase steadily with time as for the DMSO control (Fig 8C), laminin-511 coating prevented the decrease in attached cells seen between 36 and 48 hours in uncoated wells ($p = 0.0156$). These effects were absent in laminin-411 and -111-coated wells (Fig S8B-C). Laminin coating did not impact HDMEC survival in the presence or absence of mycolactone at 48 hours (Fig S8D), although as mentioned before, cell death due to mycolactone is minimal prior to 72 hours [19].

For migration, we performed a scratch assay on HUVECs in wells coated or not with laminins prior to mycolactone exposure. Monitoring cell migration using time-lapse imaging revealed that control HUVECs took less than 16 hours to close a 600-800 µm gap (Video 3). By contrast, the leading edge of wounded HUVEC monolayers exposed to mycolactone gradually stopped migrating into the cell-free region after ~7 hours; at this point the cells began to migrate randomly before undergoing the previously described morphological changes (Video 4). However, strikingly, in HUVEC monolayers plated onto laminin-511, cells continued to migrate into the gap in the presence of mycolactone, with a leading edge still evident after 16 hours (Video 5). Cell counts per unit scratch area at 8 and 16 hours showed that cells plated onto laminin-511 were able to migrate back at a rate comparable to that seen in monolayers exposed to DMSO in uncoated wells (Fig 8D, $p = 0.286$). We did not see these same effects on laminin-411 and -111-coated wells (Video 6 and 7) where migration rates remained significantly lower than the control ($p = 0.0054$ and 0.0003, respectively, Fig S8E).

This ability of laminin α5 to reverse or diminish the impact of mycolactone on endothelial cell adhesion, morphology and migration highlights the contribution of the loss of basement membrane proteins to the phenotypic changes induced by mycolactone and

presents an unanticipated potential for use in wound care in Buruli ulcer skin lesions, although such therapies are currently in their infancy [47].

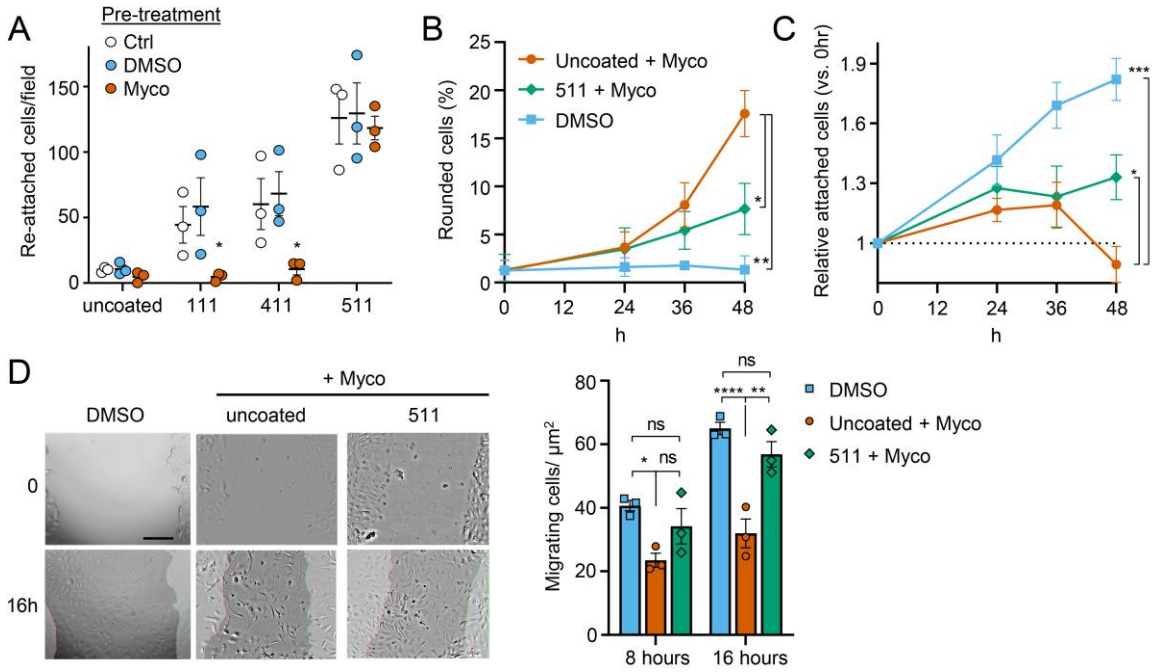

Figure 8. Laminin α5 ameliorates mycolactone-driven endothelial cell detachment and impaired migration. Endothelial cells exposed to 10 ng/mL mycolactone (Myco) or 0.02% DMSO for 24 hours or indicated times. **A**. Treated HDMECs were harvested and re-seeded to laminin-511, 411, 111 or uncoated plates. After an hour, unbound cells were washed away and attached cells were imaged and cell numbers per field are presented as mean ± SEM of 3 independent experiments. **B-D**. Endothelial cells seeded onto laminin-511 or uncoated plates were exposed to mycolactone (Myco) or DMSO. (**B-C**) HDMECs were imaged every 30 minutes over 48 hours. Rounded or attached cells per condition were counted at 0, 24, 36, 48 hours. Data are presented as a % of total cell number of each condition (**B**) or normalised to the attached cell number counted at 0 hours (**C**) (mean ± SEM of 3 independent experiments). (**D**) A scratch was introduced to a HUVEC monolayer prior to treatment. The wounded area was imaged every 15 minutes for 24 hours. Cells migrating into the original scratch area were counted at 0, 8 and 16 hours. Data are presented as cell count per scratch area (mean ± SEM of 3 independent experiments). ns, not significant; *, $P < 0.05$; **, $P < 0.01$. Statistical analysis was performed in GraphPad Prism Version 9.4.1 using 2-way ANOVA with Tukey's correction for multiple comparisons (all analysed panels; panels **B**&**C** also included the Geisser Greenhouse correction for sphericity).

Discussion

Until recently, the pathogenesis of BU was thought to rely on two factors; immunosuppression due to the action of mycolactone on innate and adaptive immunity, and direct cytotoxic action of mycolactone on the cells present within the subcutis leading to cell death and necrosis. Our findings provide further evidence supporting a third and vital pathway to tissue necrosis; the induction of endothelial dysfunction that drives an indirect mechanism leading to tissue necrosis via the breakdown of vessel integrity and fibrin-driven ischemia within tissue.

The current work reaffirms the critical role that Sec61 inhibition plays in the virulence mechanism of mycolactone. In this post-transcriptional, co-translational mechanism responsible for changes in protein abundance, proteins are made in the wrong cellular compartment (the cytoplasm) and degraded by the ubiquitin-proteasome system or removed by autophagy [7, 15]. During the current studies we tried, without success, to express examples of our library of SEC61A1 mutants that confer resistance to mycolactone [10, 17] in primary endothelial cells. This suggests that the endothelium is particularly sensitive to functional perturbation of the Sec61 translocon and perhaps explains why these cells are so exquisitely sensitive to the compound. As an alternative approach, we tested two analogues of the structurally unrelated Sec61 inhibitor Ipomoeassin F that was first isolated as a natural product of the “Morning Glory” flower [31]. Across multiple readouts, this induced comparable phenotypes to mycolactone, in the same time frame, including changes in morphology, loss of GAGs, matrisome proteins required for their synthesis, proteoglycan core proteins and basement membrane proteins. Hence, we are confident that the primary target of mycolactone in endothelial cells is Sec61, as it has already been shown in immune cells [6, 7, 14], fibroblasts [15] and epithelial cells [17]. Since epithelial cells showed similar effects on migration to those we report here, these effects probably depend on its action on the Sec61 translocon rather than other previously proposed mechanisms such as WASP activation [29].

Although the Sec61 translocon is thought to be required for the biosynthesis of approximately 30% of the proteome, mycolactone only inhibits production of specific subsets of proteins that traffic through the ER. As their depletion rate depends on protein turnover, inhibitory effects cannot be predicted *a priori*. Therefore, we performed quantitative proteomic analysis of total membrane fractions of primary endothelial cells to identify as many of the targets of mycolactone as possible, since “whole cell” approaches can bias against membrane proteins, particularly insoluble ones. Indeed, this approach was successful, more than doubling the number of detected proteins classified as membrane, secretory, ER/ERGIC, Golgi or endolysosomal compared to previous studies [12]. Significant depletion of our previously discovered targets by candidate gene approaches (including loss of CDH5, TIE-1, TEK, JAM-C, CD31, vWF, TFPI and TM [19, 20], and induction of SQSTM1/p62 [15]) validates this data set. The pattern of protein topologies affected by mycolactone reflected that seen in *in vitro* translocation assays and whole cell proteome analysis [6, 11, 12, 16, 34], further supporting mycolactone selectivity towards secreted, Type I and Type II single pass membrane proteins, with few multi-pass proteins and no Type III or tail- anchored membrane proteins showing any reduction in expression.

GO analysis confirmed induction of cytoplasmic/oxidative stress responses [17, 39, 48] amongst >220 up-regulated processes in mycolactone-exposed endothelial cells. However, in this work we focussed on the >480 down-regulated proteins, which represented a striking inadequacy in components of glycoprotein biosynthesis and metabolism and ECM organization, many of which we have validated individually. Taking together the cellular compartment analysis and our understanding of mycolactone’s cellular target, we were able to correctly hypothesise that the effects on endothelial cell function were exacerbated by loss of Golgi-localised Type II transmembrane enzymes involved in GAG (CS, DS and HS) production. Up to now, the impact of mycolactone on Golgi function has been underappreciated, but the wider ranging effect on protein glycosylation may explain why mycolactone has such a strong effect on glycosylated protein production irrespective of

topology [7]. It also suggests that the effects of mycolactone may be even more far-reaching than expected, as even molecules resistant to the Sec61 blockade at the protein level may be functionally affected due to the loss of glycosylation.

Since GAG biosynthesis is a sequential process, and the endothelial glycocalyx is essential to maintain monolayer permeability [49], we reasoned that loss of one of the GAG linker-building enzymes common to CS, DS and HS could be sufficient to explain the mycolactone-induced phenotype. This was supported by siRNA-mediated knockdown of B3GALT6, which transfers galactose to substrates such as galactose-beta-1,4-xylose, i.e. the third step in this process. B3GALT6 knockdown phenocopied the elongated appearance seen in primary endothelial cells exposed to mycolactone. The intermediate phenotype seen in some experiments suggests that depletion of junctional molecules by mycolactone [20], also plays an important contributory role. In the context of BU, it is interesting to note that children born with ‘linkeropathies’, who have a reduced ability to synthesise GAG linker regions [50, 51], display phenotypes such as skin fragility and delayed wound healing [52] that are similar to antibiotic-treated *M. ulcerans* infections. As well as increasing permeability, the loss of the glycocalyx could exacerbate the inhibition of leukocyte homing caused by mycolactone [4]. Notably other viral and bacterial pathogens promote colonisation by degrading the endothelial glycocalyx [53-55], however here the mechanism is via inducing the production of heparanase and other proteinases.

Importantly, it is not only the GAGs of the apical glycocalyx that are depleted by mycolactone. Many proteoglycan core proteins are also lost. The secretory protein perlecan is notable for being a component of the glycocalyx as well as the BM and was profoundly and rapidly lost from the surface of primary endothelial cells following mycolactone exposure. Other BM components, particularly laminins and their cellular receptors, were also found to be depleted. Excitingly, providing an exogenous coating of laminin α5-containing laminin-511 complex to tissue culture wells protected endothelial cells from mycolactone-driven changes, improving adhesion, and reversing the migration defect. We have not been

able to ascribe this to the retention of a specific adhesion molecule, and instead postulate that rescue could be via residual expression of a wide variety of laminin α5 receptors. This is supported by previous work showing that laminin α5 is more promiscuous that laminin α4 [46].

Adequate adhesion to the BM is critical for endothelial cell proliferation, migration, morphogenesis and survival [22]. Furthermore, loss of perlecan and laminin α4, or reduced binding to fibronectin, disturbs the structural integrity and maturation of microvessels [56-58], Finally, laminin α5 not only guides tissue patterning [59] and development [60] but also maintains vascular homeostasis by stabilising endothelial cell tight junctions [28]. Therefore, it is perhaps not surprising that we found the BM to be disturbed in *M. ulcerans* infected footpads. Moreover, this was seen in more advanced infections where fibrin deposition was also present within tissue, due to disturbance of the boundary between damaged vessels and dermal connective tissue. It is possible that these effects are exacerbated by IL-1β *in vivo*; this Sec61-independent pro-inflammatory cytokine has been shown to be induced in macrophages by mycolactone and *M. ulcerans* [61, 62] and is known to have profound effects on endothelial cell function, including the downregulation of anticoagulant and junctional proteins, induction of vascular permeability and upregulation of BM degrading proteinases [63]. There is considerable overlap in the endothelial cell responses to IL-1β and mycolactone, although the former's effects are mediated predominately at the transcriptional level. An additive effect of mycolactone has been shown for some of these phenotypes *in vitro* [19, 20] although the *in vivo* situation is likely more complex [62]

In summary, this study identifies loss/disruption of the endothelial glycocalyx and BM as a critical molecular process in the pathogenesis of Buruli ulcer. These effects were the same with mycolactone extracted from *M. ulcerans* bacteria and chemically synthesised material, supporting the physiological relevance of our findings. Since these changes occur prior to mycolactone-driven apoptosis [17-19], they provide further support for our working model whereby mycolactone builds a hyper-coagulative environment alongside disruption of

the endothelial monolayer and BM integrity. We propose that this leads to leakage of high molecular weight plasma proteins into the connective tissue where they activate the coagulation cascade leading to fibrin deposition and tissue ischemia. The detection of extravascular fibrinogen at early stages of infection prior to widespread tissue damage and necrosis provides further evidence that endothelial dysfunction could be a driver of disease progression. Rethinking of BU as a vascular disease may ultimately lead to improved therapies that support better wound healing, alongside antibiotic treatment. However, it should be remembered that tissue repair requires a controlled progression through a series of different stages [64]; following injury, under normal circumstances, platelet accumulation in a fibrin and fibronectin rich matrix is followed by an inflammation phase [65]. Therefore, ameliorating the coagulative features with anticoagulants alongside the standard antimycobacterial drugs may be of most value in the initial stages of treatment, while bioactive dressings containing laminin-derived peptides might be more useful to promote healing at later stages. In this context, laminin-derived bioactive peptides have recently been proposed as a treatment for defective tissue repair [47] and indeed, accelerate re-epithelialisation in wounds of diabetic animals [66, 67], suggesting this novel approach may be an effective complement to current therapies and could alleviate the long wound healing times experienced by BU patients.

Materials and methods

Key Resources Table				
Reagent type (species) or resource	**Designation**	**Source or reference**	**Identifiers**	**Additional information**
strain, strain background (include species and sex here)	C57BL/6J mouse, female	Charles River	RRID:MGI:3028467	
strain, strain background (include species and sex here)	Mu_1082 *M. ulcerans*	Richard Phillips, KCCR, Ghana		
cell line (Human primary cells)	HUVEC	PromoCell	C-12200	Single Donor
cell line (Human primary cells)	HDMEC	PromoCell	C-12210	Juvenile, Single Donor, male
antibody	Anti-fibrinogen (rabbit polyclonal)	Agilent DAKO	A0080 RRID:AB_2894406	IHC: (1:3000)
antibody	Biotinylated horse anti-rabbit IgG	Vector laboratories	BP-100-50 RRID:AB_3661924	IHC (1:50)
antibody	Anti-human Δ-HS (mouse monoclonal F69-3G10)	AMSBIO	370260-S RRID:AB_10892311	FACS (1:200) WB (1:1000)
antibody	Anti-chondroitin sulphate (mouse monoclonal CS56)	Merck	C8035 RRID:AB_476879	FACS (1:200)

antibody	Anti-perlecan (mouse monoclonal 7B5)	Thermo Fisher Scientific	13-4400 RRID:AB_86311	FACS (1:200) IFA (1:500)
antibody	Anti-glypican-1 (goat polyclonal)	Novus Biologicals	AF4519 RRID:AB_2232505	FACS (2.5µg/10^6 cells)
antibody	Anti-integrin β4/CD104 (rat monoclonal 439-9B)	eBioscience	**14-1049-82 RRID:AB_1210460**	FACS (1:100)
antibody	Anti-integrin β1/CD29 (mouse monoclonal P4C10)	Novus Biologicals	NBP2-36561 RRID:AB_3295906	FACS (1:200)
antibody	Anti-syndecan-2 (rat monoclonal 305515)	Novus Biologicals	MAB2965 RRID:AB_2182871	FACS (0.25µg/10^6 cells)
antibody	Anti-biglycan (goat polyclonal)	Novus Biologicals	AF2667 RRID:AB_2065204	FACS (0.1µg/10^6 cells)
antibody	Anti-laminin α5 (mouse monoclonal CL3118)	Novus Biologicals	NBP2-42391 RRID:AB_3306362	FACS (1:200)
antibody	Anti-laminin α4 (sheep polyclonal)	Biotechne	AF7340 RRID:AB_3644426	IFA (1:200)
antibody	Isotype control (mouse monoclonal IgG1κ P3.6.2.8.1)	Thermo Fisher Scientific (Invitrogen)	14-4714-81 RRID:AB_470110	FACS (1:100)
antibody	Isotype control (mouse IgG2b)	Thermo Fisher Scientific	MG2B00 RRID:AB_2921189	As appropriate (same as test Ab)

antibody	Isotype control (polyclonal goat IgG)	R&D Systems	AB-108-C RRID:AB_354267	As appropriate (same as test Ab)
antibody	Isotype control (rat monoclonal IgG2bκ (eB149/ 10H5)	Thermo Fisher Scientific	14-4031-81 RRID:AB_470098	As appropriate (same as test Ab)
antibody	Isotype control (mouse monoclonal IgM, clone PFR-03)	Thermo Fisher Scientific	**MA1-10438 RRID:AB_2536806**	As appropriate (same as test Ab)
antibody	PE-F(ab')2-anti-mouse IgG (rat polyclonal)	Thermo Fisher Scientific	12-4010-82 RRID:AB_11063706	As appropriate
antibody	FITC-anti-goat IgG (donkey polyclonal)	Thermo Fisher Scientific	A16000 RRID:AB_2534674	As appropriate
antibody	FITC-anti-rat IgG (goat polyclonal)	Thermo Fisher Scientific	31629 RRID:AB_228240	As appropriate
antibody	Anti-fibronectin (rabbit polyclonal)	Merck Millipore	AB1945 RRID:AB_2231910	WB (1:1000)
antibody	Anti-integrin α5 (mouse monoclonal IgG1κ A-11)	Santa Cruz Biotechnology	sc-166665 RRID:AB_2280538	WB (1 :1000)
antibody	HRP-Anti-rabbit IgG (donkey polyclonal)	GE Healthcare	NA934V RRID:AB_2722659	WB (1:5000)
antibody	HRP-Anti-mouse IgG (sheep polyclonal)	GE Healthcare	NA931V RRID:AB_772210	WB (1:5000)

antibody	Anti-B3GALT6 (mouse polyclonal)	Bio-Techne	H00126792-B01P RRID:AB_3146818	IF (1:100)
antibody	Anti-giantin (rabbit polyclonal)	Abcam	Ab80864 RRID:AB_10670397	IF (1:200)
antibody	Alexa Fluor 594 anti-rabbit IgG (goat polyclonal)	Thermo Fisher Scientific	A11012 RRID:AB_2534079	IF (1:400)
antibody	Alexa Fluor 488 anti-mouse IgG (donkey polyclonal)	Thermo Fisher Scientific	A21202 RRID:AB_141607	IF (1:400)
antibody	Alexa Fluor 488 anti-sheeo IgG (donkey polyclonal)	Thermo Fisher Scientific	A11015 RRID:AB_2534082	IF (1:500)
antibody	Alexa Fluor 647 anti-mouse IgG (goat polyclonal)	Thermo Fisher Scientific	A21235 RRID:AB_2535804	IF (1:400)
antibody	Alexa Fluor 647 anti-rabbit IgG (goat polyclonal)	Thermo Fisher Scientific	A21244 RRID:AB_2535812	IF (1:400)
sequence-based reagent	Silencer SiRNA negative control No 1	ThermoFisher Scientific	AM4611	50nM
sequence-based reagent	Human B3GALT6 siRNA	ThermoFisher Scientific	Assay ID#112321	50nM
sequence-based reagent	Human B3GALT6 siRNA	ThermoFisher Scientific	Assay ID#112322	50nM

peptide, recombinant protein	Human Laminin-111	BioLamina	LN111-02	5µg/ml
peptide, recombinant protein	Human Laminin-411	BioLamina	LN411-02	5µg/ml
peptide, recombinant protein	Human Laminin-511	BioLamina	LN511-0202	5µg/ml
peptide, recombinant protein	Human IL-1β	Gibco	PHC0813	100ng/ml
commercial assay or kit	ImmPACT NovaRED peroxidase substrate kit	Vector Laboratories	SK4805	
commercial assay or kit	VECTASTAIN Elite ABC kit	Vector Laboratories	PK6100	
chemical compound, drug	Dimethyl sulfoxide HYBRI-MAX	Merck	D2650	
chemical compound, drug	Synthetic Mycolactone		CAS: 222050-77-3	Prof Yoshito Kishi, Harvard University
chemical compound, drug	Biological Mycolactone		CAS: 222050-77-3	Dr Estelle Marion, INSERM
chemical compound, drug	Ipomoeassin F		CHEMBL4163767	Prof Wei Shi, University of Arkansas
chemical compound, drug	ZIF-80		None	Prof Wei Shi, University of Arkansas

software, algorithm	Image J (v1.52n)	Fiji		
software, algorithm	Zencell-owl software (version 3.3)	innoME GmbH		
software, algorithm	Prism Version 9.4.1	GraphPad		
software, algorithm	FlowJo v9	FlowJo.com		
other	Optimem	ThermoFisher Scientific	15392402	
other	Escort IV transfection reagent	Merck	L3287	
other	Endothelial cell growth medium 2	PromoCell	C-22011	
other	Osteosoft	Merck	1.01728	
other	Heparinase III (EC4.2.2.8 from *Flavobacterium heparinum*)	Merck	H8891	1mU/ml
other	Chondroitinase ABC (EC 4.2.2.4 from *Proteus vulgaris*)	AMSBIO	100330-1A	10mU/ml
other	TRITC-conjugated phalloidin	Merck	FAK100	1:500
other	FITC-dextran 70kDa	Merck	46945	1:500

Mycolactone and other translocation inhibitors

For all experiments in main figure panels, we used synthetic mycolactone A/B [68], which was generously donated by Prof. Yoshito Kishi (Harvard University). However, we also

compared synthetic mycolactone A/B to that extracted from cultures of *M. ulcerans* (which also makes mycolactone A/B) which was a kind gift from Dr Estelle Marion (INSERM). Here, *M. ulcerans* 1615 strain, was grown in Middlebrook 7H10 agar supplemented with Oleic Albumin Dextrose Catalase growth supplement. Bacteria were re-suspended in chloroform-methanol (2:1, v/v) and cell debris were removed after centrifugation. Folch extraction was realized by adding 0.2 volume water. The organic phase was dried and phospholipids were precipitated with ice-cold acetone. The acetone-soluble lipids were loaded on a thin layer chromatography plate and eluted with chloroform-methanol-water (90:10:1) solvent as mobile phase. The yellow band with a retention factor of 0.23 was scraped, filtered, evaporated and then resuspended in absolute ethanol. Mycolactone was stored in absolute ethanol at -20°C in the dark. The amount of purified mycolactone was determined by high-performance liquid chromatography (HPLC) on a C18 column.

Ipomoeassin F and ZIF-80 (Compound 2 in ref 30) were synthesised by Dr Wei Shi. All synthetic compounds were diluted from stock solutions in DMSO (biological mycolactone stock solution was in ethanol) and were used at the minimal inhibitory concentration, which was 10 ng/ml (~13 nM) mycolactone [15], 400nM Ipomoessin F [69] and 20nM ZIF-80 [30]. To control for potential impact of the DMSO solvent on cell function, DMSO diluted equivalently was used; typically this was 0.02%.

Cell culture and treatment

Juvenile, single donor human microvascular endothelial cells (HDMEC) and human umbilical vein endothelial cells (HUVEC) (Promocell) were cultured in hVEGF containing Endothelial cell growth medium 2 (Promocell) at 37°C and 5% CO_2. Cells were routinely seeded at a concentration of 1 x $10^4/cm^2$ in $25cm^2$ or $75cm^2$ flasks for no more than 15 population doublings. Where used, laminin-511, -411 or -111 (BioLamina, Sweden) were coated on the surface of uncoated 96-well tissue culture plates at 5 µg/mL in PBS at 4°C overnight, then

washed with medium prior to further experiment. Viability assays used either resazurin dye (Sigma Aldrich) or CellEvent (Invitrogen) as described [15, 17].

Uniaxial shear stress induction

In order to mimic the conditions of flow, we used an established technique using an orbital shaker [70]. HDMEC were grown to confluency in 6-well plates then placed on an orbital shaker rotating at 150rpm for 24 hours. Mycolactone or DMSO were added in triplicate and the cells cultured for an additional 48 hours maximum. All phase contrast and fluorescent images were taken towards the edge of the wells, where cells experience atheroprotective uniaxial shear stress [70] using an Etaluma Lumascope 620.

Time-lapse imaging of live cells

For time-lapse monitoring, endothelial cells were imaged every 30 minutes using a zenCELL Owl incubator microscope (innoME GmbH, supplied by LabLogic UK) for 48 hours. Time-lapse videos were generated with zencell-owl software (version 3.3, innoME GmbH), and analysed using their proprietary built-in algorithms of relative cell coverage, proportion of detached cells, and total cell numbers. In some cases, images of cells from certain time points were further analysed in Image J (v1.52n) to cell count of rounded cells per field, and/or the proportion and length/width ratio of elongated cells.

Scratch assay

Endothelial cells were grown to confluency in 24 well plates then single lines were scratched into the monolayer using a p20 pipette tip. Healing of HDMECs was monitored by imaging at various time points up to 24 hours. Each assay was carried out in triplicate wells. Wounded

HUVECs were monitored every 15 minutes by zenCELL Owl microscope (innoME GmbH) for up to 30 hours.

***Mycobacterium ulcerans* mouse footpad infection model**

Mycobacterium ulcerans strain Mu_1082 was cultivated on Middlebrook 7H11 agar (Merck) supplemented with 0.2% glycerol (ThermoFisher Scientific) and 10% OADC (ThermoFisher Scientific). Several days before inoculation, bacteria were scraped from the plate and resuspended in 10ml 7H9 medium (Becton Dickinson) containing 0.5% glycerol, 10% OADC and 0.2% Tween-80 (Merck) and incubated shaking with 3µm glass beads for 3 days at 31°C. To prepare the inoculum, cultures were allowed to stand for 10min (to allow clumps to settle) then 1ml culture was centrifuged at 13,000 x g for 2min. The supernatant was removed, and the pellet resuspended in Dulbecco's PBS (Fisher Scientific). After measuring the OD600, 3.33 x 10^7 bacteria were pelleted and resuspended in 10ml PBS, to give an inoculum of ~10^5 cfu/footpad in a volume of 30µl.

All *in vivo* procedures were approved by the local ethics committee and UK Home office and met relevant animal welfare and biosafety regulatory standards. In this publication we present new histological analysis of archived material from eight to nine-week-old C57BL/6J female mice (Charles River, UK), which had been inoculated intradermally with 30 µl of the bacterial suspension or vehicle control (PBS) to the left hind footpad. Mice were maintained under specific pathogen-free conditions at a temperature of 20–24 °C and humidity of 45 to 65% in individually HEPA filtered cages. The mice had free access to water and a standard balanced diet, standard bedding and enrichments including a tunnel and nesting material. Infected mice were housed separately from uninfected mice, and blinding was not possible as the infection is clearly visible. Infection grade was assessed daily according to the method of Converse [71], where Grade 1 showed swelling of the metatarsal area (<50% increase compared to normal), Grade 2 showed greater swelling (50-150%) and Grade 3 had swelling

further up the leg, visualised at the hock. Mice were killed by a schedule 1 method (cervical dislocation). The whole foot was then removed and fixed by immersion in 10% neutral buffered formalin for at least 24 hours.

Histological analysis of murine foot samples

Fixed murine feet were decalcified using the EDTA-based Osteosoft solution (Merck) and then embedded in paraffin for histological analysis.by Ziehl-Neelsen stain, Alcian blue-periodic acid Schiff stain, and immunohistochemistry (IHC) for fibrin(ogen). For IHC staining, 5-µm tissue sections on polylysine-coated slides were deparaffinised, endogenous peroxidase quenched, epitope unmasked with heated IHC citrate buffer (pH 6.0) (Merck) and blocked with 5% bovine serum albumin. The tissue sections were incubated with anti-fibrinogen antibody (A0080, DAKO) or matched isotype control overnight at 4°C. Staining was then performed with biotinylated horse anti-rabbit IgG (Vector Laboratories) and VECTASTAIN Elite ABC kit and ImmPACT NovaRED peroxidase substrate and further counterstained with Harris Haematoxylin (ThermoFisher Scientific). Whole slide images were captured using the NanoZoomer slide scanner (Hamamatsu Photonics) and analysed using ImageScope software (Leica Biosystems) and ndp2.view software (Hamamatsu). Some photographs were taken with Micropix microscope camera (acquisition software Cytocam) attached to a Yenway CX40 laboratory microscope (Micropix).

Electron microscopy

Glabrous skin from the infected hind paw of a mouse at grade 1 was dissected and freshly immersed in a fixative solution containing 4%, Formaldehyde and 3% Glutaraldehyde. After 24h, the tissue area of interest was chosen via examination of semi-thin sections of 500nm stained with toluidine blue. By using a Leica ultramicrotome with diamond knife, ultrathin sections of 100nm were collected into copper grids and images were obtained by FEI Tecnai T12.

Membrane protein preparation

HDMEC (1 x 10^7 cells) were seeded onto 15cm dishes (Corning) and grown to 90% confluency then exposed to solvent carrier DMSO or 10ng/ml mycolactone for 24 hours. Cells were washed four times in PBS and once in lysis buffer (10mM Tris pH 7.5, 250mM Sucrose, protease inhibitor cocktail). Cells were incubated for 20min on ice in 10ml lysis buffer then lysed in by 20 strokes dounce homogenisation. Lysates were centrifuged at 1,000x*g* for 10min at 4°C then the post-nuclear supernatant was centrifuged at 100,000x*g* for 1 hour at 4°C. Pellets were resuspended in 110 µl lysis buffer. Protein concentration was determined by BCA assay and 50 µg aliquots were subjected to acetone precipitation. Triplicate samples were prepared from 3 independent assays.

Proteomics

Acetone precipitated proteins were reduced, alkylated and digested with trypsin before 9-plex isobaric TMT labelling according to the manufacturer's protocol (https://www.thermofisher.com/document-connect/document-connect.html?url=https://assets.thermofisher.com/TFS-Assets%2FLSG%2Fmanuals%2FMAN0016969_2162457_TMT10plex_UG.pdf). Labelled peptides were separated by high pH reverse phase liquid chromatography, collecting 20 fractions which were then lyophilised, desalted and analysed by LC-MS/MS. TMT labelled samples were analysed by the SPS-MP3 method using an Orbitrap Lumos mass spectrometer. Spectra were searched using the Mascot search engine version (Matrix Science) and analysed using the Proteome Discovery platform. (Version 2.2ThermoFisher Scientific). NA values and low confidence proteins were removed, and data was normalised using each channel median. Differential expression analysis was carried out using Limma. Adjusted p values were calculated by the Benjamini-Hochberg method. UniProt and the Human Protein Atlas (https://www.proteinatlas.org) were used to determine protein location

and characteristics. Over-representation of GO groups was assessed using Webgestalt (www.webgestalt.org). Signal peptide ΔG values were obtained via the ΔG Prediction Server V1.0 (https://dgpred.cbr.su.se). The mass spectrometry proteomics data have been deposited to the ProteomeXchange Consortium via the PRIDE [72] partner repository with the dataset identifier PXD037489.

siRNA transfection

HUVECs (2 x 10^5 cells) were seeded onto a 6-well plate. The next day, cells were washed with Opti-MEM (Gibco) and then kept in 1 ml medium. Each siRNA (Silencer siRNA assays ID#112321, #112322 for B3GALT6 or Silencer negative control No.1 siRNA AM4611; Invitrogen ThermoFisher Scientific) was diluted in Opti-MEM to 0.6 μM, mixed with equal volume of diluted Escort IV transfection reagent (L3287, Merck; final concentration 60 μg/mL). The transfection was performed onto HUVECs with ~40% confluency. Medium was changed back to normal endothelial culture medium 5 hours later. The transfectants received treatment 24-hour post transfection and subjected to the respective analysis (e.g., image, sample harvest for immunochemical assays) after another 24 hours.

Flow cytometry

Flow cytometry was carried out according to standard methods as described in [19] using an Attune NxT flow cytometer (ThermoFisher Scientific). Cells were detached with non-enzymatic cell dissociation solution (Merck) or briefly (for Itgb4 staining only) trypsinised with 0.04% trypsin/ 0.03% EDTA (PromoCell). For surface GAG detection, cells were treated with 1mU of heparinase III (EC4.2.2.8 from *Flavobacterium heparinum*) to expose neo-epitope of heparan sulphate or with chondroitinase ABC (EC 4.2.2.4 from *Proteus vulgaris*) (AMS Biotechnology) for 1h at 37°C prior to the staining procedures. Antibodies were Δ-HS (F69-3G10, AMS Biotechnology), CS (CS56, Merck), perlecan (7B5, ThermoFisher Scientific),

glypican-1 (AF4519), integrin β4/ CD104 (clone 439-9B, eBioscience), integrin β1/ CD29 (P4C10, NBP2-36561), syndecan-2 (MAB2965), biglycan (AF2667), laminin α5 (NBP2-42391) from Biotechne. Isotype control mouse IgG1 (P3.6.2.8.1; 14-4714-81 from Invitrogen), mouse IgG2b (MG2B00), goat IgG (AB-108-C from R&D), rat IgG2b (14-4031-81), mouse IgM (PFR-03) and fluorophore-conjugated secondary antibodies goat anti-mouse IgG PE (12-4010-82), donkey anti-goat IgG FITC (A16000) and anti-rat IgG FITC (31629) were from ThermoFisher Scientific. The main population was gated by forward and side scatter plot of untreated cells using FlowJo (v9); among this, single cell population of 10^4 cells per condition was subjected to analysis. Mean fluorescence intensity was determined and presented as % relative to untreated control.

Immunoblotting

Immunoblotting was carried out according to standard methods as described in [19]. Endothelial cells were lysed either in RIPA buffer (where protein content-equalised post-nuclear fractions were used) or directly in 'gel sample buffer' (with sonication to degrade genomic DNA). Immunoblotting of commercial pre-cast gels (BioRad) used either Immobilon PVDF membranes (Merck) or nitrocellulose membrane (GE Healthcare). Antibodies used in this study were: Δ-HS (F69-3G10, AMS Biotechnology); anti-fibronectin (AB1945, Merck); anti-integrin α5 (sc-166665); anti-rabbit-HRP (GE Healthcare, NA934V), anti-mouse-HRP (GE Healthcare, NA931V). To visualise HS neoepitope, protein lysate was digested with 1 mU of heparinase III (EC4.2.2.8 from *Flavobacterium heparinum*) prior to SDS-PAGE.

Immunofluorescence

Immunofluorescent imaging was carried out according to standard methods as described in [15]. Cells were fixed with 4% paraformaldehyde in PBS. For visualising intracellular markers, cells were permeabilised wit 0.25% Nonidet P-40 alternative in NETGEL buffer (150 mM NaCl, 5mM EDTA, 50 mM Tris-Cl, pH 7.4, 0.05% Nonidet P-40 alternative, 0.25%

gelatin and 0.02% sodium azide). Antibodies used in this study were: B3GALT6 (H00126792-B01P, Biotechne), Giantin (ab80864, abcam), Laminin α4 (AF7340, Biotechne), Δ-HS (F69-3G10, AMS Biotechnology), perlecan (7B5, ThermoFisher Scientific), TRITC-conjugated phalloidin (FAK100, Merck), Alexa Fluor 594 goat anti-rabbit (A11012), Alexa Fluor 488 donkey anti-mouse (A21202) and Alexa Fluor 488 donkey anti-sheep (A11015) from Invitrogen/ThermoFisher Scientific. For B3GALT6 intensity in Golgi apparatus, the region of interest per cell was defined by giantin-positive staining using ImageJ selection tools. The integrated density of B3GALT6 fluorescence of selected regions and background reading were then measured and the difference between the two numbers were corrected total cell fluorescence.

Vascular permeability assay

Endothelial cells were seeded on hanging cell culture inserts containing 1 µm pores with a polyethylene terephthalate membrane (Falcon). Treatment as above or with 100 ng/mL IL-1β (Gibco) were applied to both the insert and receiver wells. After indicated time, fluorescein isothiocyanate (FITC)-conjugated dextran (70 kDa, Millipore) was applied to each insert for 20 minutes. The fluorescence intensity of the solution in the receiver wells was then assessed by a fluorescent plate reader (FLUOstar Omega, BMG Labtech) with excitation/ emission wavelength at 485/ 530 nm. Fluorescence intensity was normalised to untreated control wells with an intact monolayer of endothelial cells and expressed as a % of subtracted value obtained from wells where no cells were seeded to the insert.

Adhesion assay

HDMECs were harvested, incubated with anti-integrin β1 (clone P4C10, NBP2-36561, Biotechne) or isotype control mouse IgG1 (P3.6.2.8.1; 14-4714-81 from Invitrogen) for 5 minutes, then 1.5 x 10^4 cells were added to the wells of a 96 well plate that had been coated

or not with different laminins as described above. After 1 hour, each well was washed three times with serum free medium and attached cells were imaged with a digital microscope camera (Micropix) attached to an AE31E inverted microscope (Motic). The cell count per image was determined using ImageJ.

Statistical analysis

All data, with exception of the live-cell imaging using the ZenCell OWL (see above), were analysed using GraphPad Prism Version 9.4.1. Data were analysed using a one- or two-way ANOVA using an appropriate correction for multiple comparisons (either Dunnett's, or Tukey's). Some two-way ANOVAs also included the Geisser Greenhouse correction for sphericity.

Acknowledgements

We are extremely grateful to Prof Yoshito Kishi (Harvard University, USA) for the gift of synthetic mycolactone A/B. We dedicate this paper to the memory of this tremendous scientist who did some much to advance research into the pathogenesis of Buruli ulcer. We thank Dr Estelle Marion (Inserm U1302 INCIT, Angers, France) for the biologically purified mycolactone, and Prof Richard Phillips (Kumasi Centre for Collaborative Research in Tropical Medicine) who provided the *M. ulcerans* strain used in this work. We thank Katherine Walker and Ella May of the University of Surrey's Veterinary Pathology Centre for their assistance with tissue processing and staining of murine samples, and Dr Paola Campagnola (University of Surrey) for her advice in setting up the endothelial cells under flow. This work is supported by a Wellcome Trust Investigator Award in Science to Prof Rachel Simmonds (WT202843/Z/16/Z). Chemical synthesis of Ipomoeassin F and ZIF-80 was supported by an AREA grant GM116032 from the National Institute of General Medical Sciences of the National Institutes of Health (NIH) to Prof Wei Q Shi.

Additional Files

Supplementary File 1

Supplementary figures (found at the end of this PDF).

Supplementary File 2

HDMEC membrane fraction raw peptide data.

Supplementary File 3

Normalised differential expression analysis for membrane fractions of HDMEC incubated for 24 hours with DMSO vs Mycolactone

Supplementary File 4

HDMEC membrane fraction proteins significantly downregulated by mycolactone.

Supplementary File 5

HDMEC membrane fraction proteins significantly upregulated by mycolactone.

Video 1. HDMECs were exposed to 10 ng/mL mycolactone. Live cell imaging was performed with using the zenCELL Owl incubator microscope every 30 minutes for 48 hours. Time-lapse videos (representative of 3 independent experiments) were generated with zencell-owl software. Time stamp and scale bar as indicated.

Video 2. HDMECs were exposed to 0.02% DMSO. Live cell imaging was performed with using the zenCELL Owl incubator microscope every 30 minutes for 48 hours. Time-lapse videos (representative of 3 independent experiments) were generated with zencell-owl software. Time stamp and scale bar as indicated.

Video 3. A scratch was introduced to HUVEC monolayer exposed to 0.02% DMSO and live cell imaging was performed with the zenCELL Owl incubator microscope every 15 min for 23 hours. Time-lapse videos (representative of 3 independent experiments) were generated with zencell-owl software. Time stamp and scale bar as indicated.

Video 4. A scratch was introduced to HUVEC monolayer exposed to 10 ng/mL mycolactone and live cell imaging was performed with the zenCELL Owl incubator microscope every 15 min for 23 hours. Time-lapse videos (representative of 3 independent experiments) were generated with zencell-owl software. Time stamp and scale bar as indicated.

Video 5. HUVECs were seeded on to laminin-511 coated well. The following day, a scratch was introduced to the monolayer and the cells were exposed to 10 ng/mL mycolactone. Live

cell imaging was then performed with the zenCELL Owl incubator microscope every 15 min for 23 hours. Time-lapse videos (representative of 3 independent experiments) were generated with zencell-owl software. Time stamp and scale bar as indicated.

Video 6. HUVECs were seeded on to laminin-411 coated well. The following day, a scratch was introduced to the monolayer and the cells were exposed to 10 ng/mL mycolactone. Live cell imaging was then performed with the zenCELL Owl incubator microscope every 15 min for 23 hours. Time-lapse videos (representative of 3 independent experiments) were generated with zencell-owl software. Time stamp and scale bar as indicated.

Video 7. HUVECs were seeded on to laminin-111 coated well. The following day, a scratch was introduced to the monolayer and the cells were exposed to 10 ng/mL mycolactone. Live cell imaging was then performed with the zenCELL Owl incubator microscope every 15 min for 23 hours. Time-lapse videos (representative of 3 independent experiments) were generated with zencell-owl software. Time stamp and scale bar as indicated.

References

1. Yotsu RR, Suzuki K, Simmonds RE, Bedimo R, Ablordey A, Yeboah-Manu D, et al. Buruli Ulcer: a Review of the Current Knowledge. Curr Trop Med Rep. 2018;5(4):247-56. Epub 2018/11/22. doi: 10.1007/s40475-018-0166-2.
2. George KM, Chatterjee D, Gunawardana G, Welty D, Hayman J, Lee R, et al. Mycolactone: a polyketide toxin from Mycobacterium ulcerans required for virulence. Science. 1999;283(5403):854-7. Epub 1999/02/05. doi: 10.1126/science.283.5403.854.
3. Sarfo FS, Phillips R, Wansbrough-Jones M, Simmonds RE. Recent advances: role of mycolactone in the pathogenesis and monitoring of Mycobacterium ulcerans infection/Buruli ulcer disease. Cell Microbiol. 2016;18(1):17-29. doi: 10.1111/cmi.12547.
4. Guenin-Mace L, Carrette F, Asperti-Boursin F, Le Bon A, Caleechurn L, Di Bartolo V, et al. Mycolactone impairs T cell homing by suppressing microRNA control of L-selectin expression. Proc Natl Acad Sci U S A. 2011;108(31):12833-8. Epub 2011/07/20. doi: 10.1073/pnas.1016496108.
5. Simmonds RE, Lali FV, Smallie T, Small PL, Foxwell BM. Mycolactone inhibits monocyte cytokine production by a posttranscriptional mechanism. J Immunol. 2009;182(4):2194-202. Epub 2009/02/10. doi: 10.4049/jimmunol.0802294.
6. Baron L, Paatero AO, Morel JD, Impens F, Guenin-Mace L, Saint-Auret S, et al. Mycolactone subverts immunity by selectively blocking the Sec61 translocon. J Exp Med. 2016;213(13):2885-96. Epub 2016/11/09. doi: 10.1084/jem.20160662.
7. Hall BS, Hill K, McKenna M, Ogbechi J, High S, Willis AE, et al. The pathogenic mechanism of the Mycobacterium ulcerans virulence factor, mycolactone, depends on blockade of protein translocation into the ER. PLoS Pathog. 2014;10(4):e1004061. Epub 2014/04/05. doi: 10.1371/journal.ppat.1004061.
8. O'Keefe S, Pool MR, High S. Membrane protein biogenesis at the ER: the highways and byways. Febs j. 2021. Epub 2021/05/08. doi: 10.1111/febs.15905.
9. Voorhees RM, Hegde RS. Structure of the Sec61 channel opened by a signal sequence. Science. 2016;351(6268):88-91. Epub 2016/01/02. doi: 10.1126/science.aad4992.
10. Gerard SF, Hall BS, Zaki AM, Corfield KA, Mayerhofer PU, Costa C, et al. Structure of the Inhibited State of the Sec Translocon. Mol Cell. 2020;79(3):406-15 e7. Epub 2020/07/22. doi: 10.1016/j.molcel.2020.06.013.
11. McKenna M, Simmonds RE, High S. Mycolactone reveals the substrate-driven complexity of Sec61-dependent transmembrane protein biogenesis. J Cell Sci. 2017;130(7):1307-20. Epub 2017/02/22. doi: 10.1242/jcs.198655.
12. Morel JD, Paatero AO, Wei J, Yewdell JW, Guenin-Mace L, Van Haver D, et al. Proteomics Reveals Scope of Mycolactone-mediated Sec61 Blockade and Distinctive Stress Signature. Mol Cell Proteomics. 2018;17(9):1750-65. Epub 2018/06/20. doi: 10.1074/mcp.RA118.000824.
13. O'Keefe S, Zong G, Duah KB, Andrews LE, Shi WQ, High S. An alternative pathway for membrane protein biogenesis at the endoplasmic reticulum. Commun Biol. 2021;4(1):828. Epub 2021/07/03. doi: 10.1038/s42003-021-02363-z.
14. Grotzke JE, Kozik P, Morel JD, Impens F, Pietrosemoli N, Cresswell P, et al. Sec61 blockade by mycolactone inhibits antigen cross-presentation independently of endosome-to-cytosol export. Proc Natl Acad Sci U S A. 2017;114(29):E5910-E9. Epub 2017/07/07. doi: 10.1073/pnas.1705242114.
15. Hall BS, Dos Santos SJ, Hsieh LT, Manifava M, Ruf MT, Pluschke G, et al. Inhibition of the SEC61 translocon by mycolactone induces a protective autophagic response controlled by EIF2S1-dependent translation that does not require ULK1 activity. Autophagy. 2021:1-19. Epub 2021/08/24. doi: 10.1080/15548627.2021.1961067.
16. Gama JB, Ohlmeier S, Martins TG, Fraga AG, Sampaio-Marques B, Carvalho MA, et al. Proteomic analysis of the action of the Mycobacterium ulcerans toxin mycolactone: targeting host cells cytoskeleton and collagen. PLoS Negl Trop Dis. 2014;8(8):e3066. Epub 2014/08/08. doi: 10.1371/journal.pntd.0003066.

17. Ogbechi J, Hall BS, Sbarrato T, Taunton J, Willis AE, Wek RC, et al. Inhibition of Sec61-dependent translocation by mycolactone uncouples the integrated stress response from ER stress, driving cytotoxicity via translational activation of ATF4. Cell Death Dis. 2018;9(3):397. Epub 2018/03/16. doi: 10.1038/s41419-018-0427-y.
18. Bieri R, Scherr N, Ruf MT, Dangy JP, Gersbach P, Gehringer M, et al. The Macrolide Toxin Mycolactone Promotes Bim-Dependent Apoptosis in Buruli Ulcer through Inhibition of mTOR. ACS Chem Biol. 2017;12(5):1297-307. Epub 20170327. doi: 10.1021/acschembio.7b00053.
19. Ogbechi J, Ruf MT, Hall BS, Bodman-Smith K, Vogel M, Wu HL, et al. Mycolactone-Dependent Depletion of Endothelial Cell Thrombomodulin Is Strongly Associated with Fibrin Deposition in Buruli Ulcer Lesions. PLoS Pathog. 2015;11(7):e1005011. Epub 2015/07/17. doi: 10.1371/journal.ppat.1005011.
20. Hsieh LT, Dos Santos SJ, Hall BS, Ogbechi J, Loglo AD, Salguero FJ, et al. Aberrant stromal tissue factor localisation and mycolactone-driven vascular dysfunction, exacerbated by IL-1beta, are linked to fibrin formation in Buruli ulcer lesions. PLoS Pathog. 2022;18(1):e1010280. Epub 2022/02/01. doi: 10.1371/journal.ppat.1010280.
21. Butenas S, Orfeo T, Mann KG. Tissue factor in coagulation: Which? Where? When? Arterioscler Thromb Vasc Biol. 2009;29(12):1989-96. Epub 2009/07/14. doi: 10.1161/ATVBAHA.108.177402.
22. Davis GE, Senger DR. Endothelial extracellular matrix: biosynthesis, remodeling, and functions during vascular morphogenesis and neovessel stabilization. Circ Res. 2005;97(11):1093-107. Epub 2005/11/25. doi: 10.1161/01.RES.0000191547.64391.e3.
23. Wallez Y, Huber P. Endothelial adherens and tight junctions in vascular homeostasis, inflammation and angiogenesis. Biochim Biophys Acta. 2008;1778(3):794-809. Epub 2007/10/27. doi: 10.1016/j.bbamem.2007.09.003.
24. Zeng Y, Ebong EE, Fu BM, Tarbell JM. The structural stability of the endothelial glycocalyx after enzymatic removal of glycosaminoglycans. PLoS One. 2012;7(8):e43168. Epub 2012/08/21. doi: 10.1371/journal.pone.0043168.
25. Reitsma S, Slaaf DW, Vink H, van Zandvoort MA, oude Egbrink MG. The endothelial glycocalyx: composition, functions, and visualization. Pflugers Arch. 2007;454(3):345-59. Epub 2007/01/27. doi: 10.1007/s00424-007-0212-8.
26. Yilmaz O, Afsar B, Ortiz A, Kanbay M. The role of endothelial glycocalyx in health and disease. Clin Kidney J. 2019;12(5):611-9. Epub 2019/10/05. doi: 10.1093/ckj/sfz042.
27. Yousif LF, Di Russo J, Sorokin L. Laminin isoforms in endothelial and perivascular basement membranes. Cell Adh Migr. 2013;7(1):101-10. Epub 2012/12/25. doi: 10.4161/cam.22680.
28. Song J, Zhang X, Buscher K, Wang Y, Wang H, Di Russo J, et al. Endothelial Basement Membrane Laminin 511 Contributes to Endothelial Junctional Tightness and Thereby Inhibits Leukocyte Transmigration. Cell Rep. 2017;18(5):1256-69. Epub 2017/02/02. doi: 10.1016/j.celrep.2016.12.092.
29. Guenin-Mace L, Veyron-Churlet R, Thoulouze MI, Romet-Lemonne G, Hong H, Leadlay PF, et al. Mycolactone activation of Wiskott-Aldrich syndrome proteins underpins Buruli ulcer formation. J Clin Invest. 2013;123(4):1501-12. Epub 2013/04/04. doi: 10.1172/JCI66576.
30. Zong G, Hu Z, Duah KB, Andrews LE, Zhou J, O'Keefe S, et al. Ring Expansion Leads to a More Potent Analogue of Ipomoeassin F. J Org Chem. 2020;85(24):16226-35. Epub 2020/12/03. doi: 10.1021/acs.joc.0c01659.
31. Zong G, Hu Z, O'Keefe S, Tranter D, Iannotti MJ, Baron L, et al. Ipomoeassin F Binds Sec61alpha to Inhibit Protein Translocation. J Am Chem Soc. 2019;141(21):8450-61. Epub 2019/05/07. doi: 10.1021/jacs.8b13506.
32. Pauwels E, Schulein R, Vermeire K. Inhibitors of the Sec61 Complex and Novel High Throughput Screening Strategies to Target the Protein Translocation Pathway. Int J Mol Sci. 2021;22(21). Epub 2021/11/14. doi: 10.3390/ijms222112007.

33. Demangel C, High S. Sec61 blockade by mycolactone: A central mechanism in Buruli ulcer disease. Biol Cell. 2018;110(11):237-48. Epub 2018/07/29. doi: 10.1111/boc.201800030.
34. McKenna M, Simmonds RE, High S. Mechanistic insights into the inhibition of Sec61-dependent co- and post-translational translocation by mycolactone. J Cell Sci. 2016;129(7):1404-15. Epub 2016/02/13. doi: 10.1242/jcs.182352.
35. Smalinskaitė L, Kim MK, Lewis AJO, Keenan RJ, Hegde RS. Mechanism of an intramembrane chaperone for multipass membrane proteins. Nature. 2022;611(7934):161-6. Epub 2022/10/20. doi: 10.1038/s41586-022-05336-2.
36. Sundaram A, Yamsek M, Zhong F, Hooda Y, Hegde RS, Keenan RJ. Substrate-driven assembly of a translocon for multipass membrane proteins. Nature. 2022;611(7934):167-72. Epub 2022/10/20. doi: 10.1038/s41586-022-05330-8.
37. Nguyen D, Stutz R, Schorr S, Lang S, Pfeffer S, Freeze HH, et al. Proteomics reveals signal peptide features determining the client specificity in human TRAP-dependent ER protein import. Nat Commun. 2018;9(1):3765. Epub 2018/09/16. doi: 10.1038/s41467-018-06188-z.
38. Schorr S, Nguyen D, Hassdenteufel S, Nagaraj N, Cavalie A, Greiner M, et al. Identification of signal peptide features for substrate specificity in human Sec62/Sec63-dependent ER protein import. FEBS J. 2020;287(21):4612-40. Epub 2020/03/07. doi: 10.1111/febs.15274.
39. Forster B, Demangel C, Thye T. Mycolactone induces cell death by SETD1B-dependent degradation of glutathione. PLoS Negl Trop Dis. 2020;14(10):e0008709. Epub 2020/10/03. doi: 10.1371/journal.pntd.0008709.
40. Gronberg A, Zettergren L, Bergh K, Stahle M, Heilborn J, Angeby K, et al. Antioxidants protect keratinocytes against M. ulcerans mycolactone cytotoxicity. PLoS One. 2010;5(11):e13839. Epub 2010/11/17. doi: 10.1371/journal.pone.0013839.
41. Bardou P, Mariette J, Escudie F, Djemiel C, Klopp C. jvenn: an interactive Venn diagram viewer. BMC Bioinformatics. 2014;15:293. Epub 2014/09/02. doi: 10.1186/1471-2105-15-293.
42. Kikegawa T, Yamaguchi T, Nambu R, Etchuya K, Ikeda M, Mukai Y. Signal-anchor sequences are an essential factor for the Golgi-plasma membrane localization of type II membrane proteins. Biosci Biotechnol Biochem. 2018;82(10):1708-14. Epub 2018/06/19. doi: 10.1080/09168451.2018.1484272.
43. Owens RT, Wagner WD. Metabolism and turnover of cell surface-associated heparan sulfate proteoglycan and chondroitin sulfate proteoglycan in normal and cholesterol-enriched macrophages. Arterioscler Thromb. 1991;11(6):1752-8. Epub 1991/11/01. doi: 10.1161/01.atv.11.6.1752.
44. Yanagishita M, Hascall VC. Proteoglycans synthesized by rat ovarian granulosa cells in culture. Isolation, fractionation, and characterization of proteoglycans associated with the cell layer. J Biol Chem. 1984;259(16):10260-9. Epub 1984/08/25.
45. Sixt M, Engelhardt B, Pausch F, Hallmann R, Wendler O, Sorokin LM. Endothelial cell laminin isoforms, laminins 8 and 10, play decisive roles in T cell recruitment across the blood-brain barrier in experimental autoimmune encephalomyelitis. J Cell Biol. 2001;153(5):933-46. Epub 2001/05/31. doi: 10.1083/jcb.153.5.933.
46. Di Russo J, Luik AL, Yousif L, Budny S, Oberleithner H, Hofschröer V, et al. Endothelial basement membrane laminin 511 is essential for shear stress response. Embo j. 2017;36(2):183-201. Epub 2016/12/13. doi: 10.15252/embj.201694756.
47. Iorio V, Troughton LD, Hamill KJ. Laminins: Roles and Utility in Wound Repair. Adv Wound Care (New Rochelle). 2015;4(4):250-63. doi: 10.1089/wound.2014.0533.
48. Kwaffo YA, Sarpong-Duah M, Owusu-Boateng K, Gbewonyo WS, Adjimani JP, Mosi L. Natural antioxidants attenuate mycolactone toxicity to RAW 264.7 macrophages. Exp Biol Med (Maywood). 2021;246(17):1884-94. Epub 2021/05/27. doi: 10.1177/15353702211015628.

49. Harding IC, Mitra R, Mensah SA, Nersesyan A, Bal NN, Ebong EE. Endothelial barrier reinforcement relies on flow-regulated glycocalyx, a potential therapeutic target. Biorheology. 2019;56(2-3):131-49. Epub 2019/04/17. doi: 10.3233/BIR-180205.
50. Colman M, Van Damme T, Steichen-Gersdorf E, Laccone F, Nampoothiri S, Syx D, et al. The clinical and mutational spectrum of B3GAT3 linkeropathy: two case reports and literature review. Orphanet J Rare Dis. 2019;14(1):138. Epub 2019/06/15. doi: 10.1186/s13023-019-1110-9.
51. Mihalic Mosher T, Zygmunt DA, Koboldt DC, Kelly BJ, Johnson LR, McKenna DS, et al. Expansion of B4GALT7 linkeropathy phenotype to include perinatal lethal skeletal dysplasia. Eur J Hum Genet. 2019;27(10):1569-77. Epub 2019/07/07. doi: 10.1038/s41431-019-0464-8.
52. Malfait F, Kariminejad A, Van Damme T, Gauche C, Syx D, Merhi-Soussi F, et al. Defective initiation of glycosaminoglycan synthesis due to B3GALT6 mutations causes a pleiotropic Ehlers-Danlos-syndrome-like connective tissue disorder. Am J Hum Genet. 2013;92(6):935-45. Epub 2013/05/15. doi: 10.1016/j.ajhg.2013.04.016.
53. Puerta-Guardo H, Glasner DR, Harris E. Dengue Virus NS1 Disrupts the Endothelial Glycocalyx, Leading to Hyperpermeability. PLoS Pathog. 2016;12(7):e1005738. Epub 2016/07/16. doi: 10.1371/journal.ppat.1005738.
54. Chiu HM, Chiou WY, Hsu WJ, Wu LH, Yang MH, Tyan YC, et al. Salmonella alters heparanase expression and reduces tumor metastasis. Int J Med Sci. 2021;18(13):2981-9. Epub 2021/07/06. doi: 10.7150/ijms.60281.
55. Tang L, Tang B, Lei Y, Yang M, Wang S, Hu S, et al. Helicobacter pylori-Induced Heparanase Promotes H. pylori Colonization and Gastritis. Front Immunol. 2021;12:675747. Epub 2021/07/06. doi: 10.3389/fimmu.2021.675747.
56. Thyboll J, Kortesmaa J, Cao R, Soininen R, Wang L, Iivanainen A, et al. Deletion of the laminin alpha4 chain leads to impaired microvessel maturation. Mol Cell Biol. 2002;22(4):1194-202. Epub 2002/01/26. doi: 10.1128/MCB.22.4.1194-1202.2002.
57. Gustafsson E, Almonte-Becerril M, Bloch W, Costell M. Perlecan maintains microvessel integrity in vivo and modulates their formation in vitro. PLoS One. 2013;8(1):e53715. Epub 2013/01/16. doi: 10.1371/journal.pone.0053715.
58. Nicosia RF, Bonanno E, Smith M. Fibronectin promotes the elongation of microvessels during angiogenesis in vitro. J Cell Physiol. 1993;154(3):654-61. Epub 1993/03/01. doi: 10.1002/jcp.1041540325.
59. Spenle C, Simon-Assmann P, Orend G, Miner JH. Laminin alpha5 guides tissue patterning and organogenesis. Cell Adh Migr. 2013;7(1):90-100. Epub 2012/10/19. doi: 10.4161/cam.22236.
60. Miner JH, Cunningham J, Sanes JR. Roles for laminin in embryogenesis: exencephaly, syndactyly, and placentopathy in mice lacking the laminin alpha5 chain. J Cell Biol. 1998;143(6):1713-23. Epub 1998/12/16. doi: 10.1083/jcb.143.6.1713.
61. Foulon M, Robbe-Saule M, Manry J, Esnault L, Boucaud Y, Alcaïs A, et al. Mycolactone toxin induces an inflammatory response by targeting the IL-1β pathway: Mechanistic insight into Buruli ulcer pathophysiology. PLoS Pathog. 2020;16(12):e1009107. Epub 2020/12/19. doi: 10.1371/journal.ppat.1009107.
62. Hall BS, Hsieh LT, Sacre S, Simmonds RE. The One That Got Away: How Macrophage-Derived IL-1β Escapes the Mycolactone-Dependent Sec61 Blockade in Buruli Ulcer. Front Immunol. 2021;12:788146. Epub 2022/02/15. doi: 10.3389/fimmu.2021.788146.
63. Cottam DW, Corbitt RH, Gomez DE, Rees RC, Thorgeirsson UP. Alterations in endothelial cell proteinase and inhibitor polarized secretion following treatment with interleukin-1, phorbol ester, and human melanoma cell conditioned medium. J Cell Biochem. 1996;60(1):148-60. Epub 1996/01/01. doi: 10.1002/(sici)1097-4644(19960101)60:1<148::aid-jcb17>3.0.co;2-l.
64. Barker TH, Engler AJ. The provisional matrix: setting the stage for tissue repair outcomes. Matrix Biol. 2017;60-61:1-4. Epub 2017/05/22. doi: 10.1016/j.matbio.2017.04.003.

65. Clark RA, Lanigan JM, DellaPelle P, Manseau E, Dvorak HF, Colvin RB. Fibronectin and fibrin provide a provisional matrix for epidermal cell migration during wound reepithelialization. J Invest Dermatol. 1982;79(5):264-9. Epub 1982/11/01. doi: 10.1111/1523-1747.ep12500075.
66. Zhu Y, Cankova Z, Iwanaszko M, Lichtor S, Mrksich M, Ameer GA. Potent laminin-inspired antioxidant regenerative dressing accelerates wound healing in diabetes. Proc Natl Acad Sci U S A. 2018;115(26):6816-21. Epub 2018/06/13. doi: 10.1073/pnas.1804262115.
67. Ishihara J, Ishihara A, Fukunaga K, Sasaki K, White MJV, Briquez PS, et al. Laminin heparin-binding peptides bind to several growth factors and enhance diabetic wound healing. Nature Communications. 2018;9(1):2163. doi: 10.1038/s41467-018-04525-w.
68. Song F, Fidanze S, Benowitz AB, Kishi Y. Total synthesis of the mycolactones. Org Lett. 2002;4(4):647-50. doi: 10.1021/ol0172828.
69. Zong G, Barber E, Aljewari H, Zhou J, Hu Z, Du Y, et al. Total Synthesis and Biological Evaluation of Ipomoeassin F and Its Unnatural 11R-Epimer. J Org Chem. 2015;80(18):9279-91. Epub 2015/09/01. doi: 10.1021/acs.joc.5b01765.
70. Warboys CM, Ghim M, Weinberg PD. Understanding mechanobiology in cultured endothelium: A review of the orbital shaker method. Atherosclerosis. 2019;285:170-7. Epub 2019/05/17. doi: 10.1016/j.atherosclerosis.2019.04.210.
71. Converse PJ, Nuermberger EL, Almeida DV, Grosset JH. Treating Mycobacterium ulcerans disease (Buruli ulcer): from surgery to antibiotics, is the pill mightier than the knife? Future Microbiol. 2011;6(10):1185-98. doi: 10.2217/fmb.11.101.
72. Perez-Riverol Y, Bai J, Bandla C, García-Seisdedos D, Hewapathirana S, Kamatchinathan S, et al. The PRIDE database resources in 2022: a hub for mass spectrometry-based proteomics evidences. Nucleic Acids Res. 2022;50(D1):D543-d52. Epub 2021/11/02. doi: 10.1093/nar/gkab1038.

Supplementary Figures

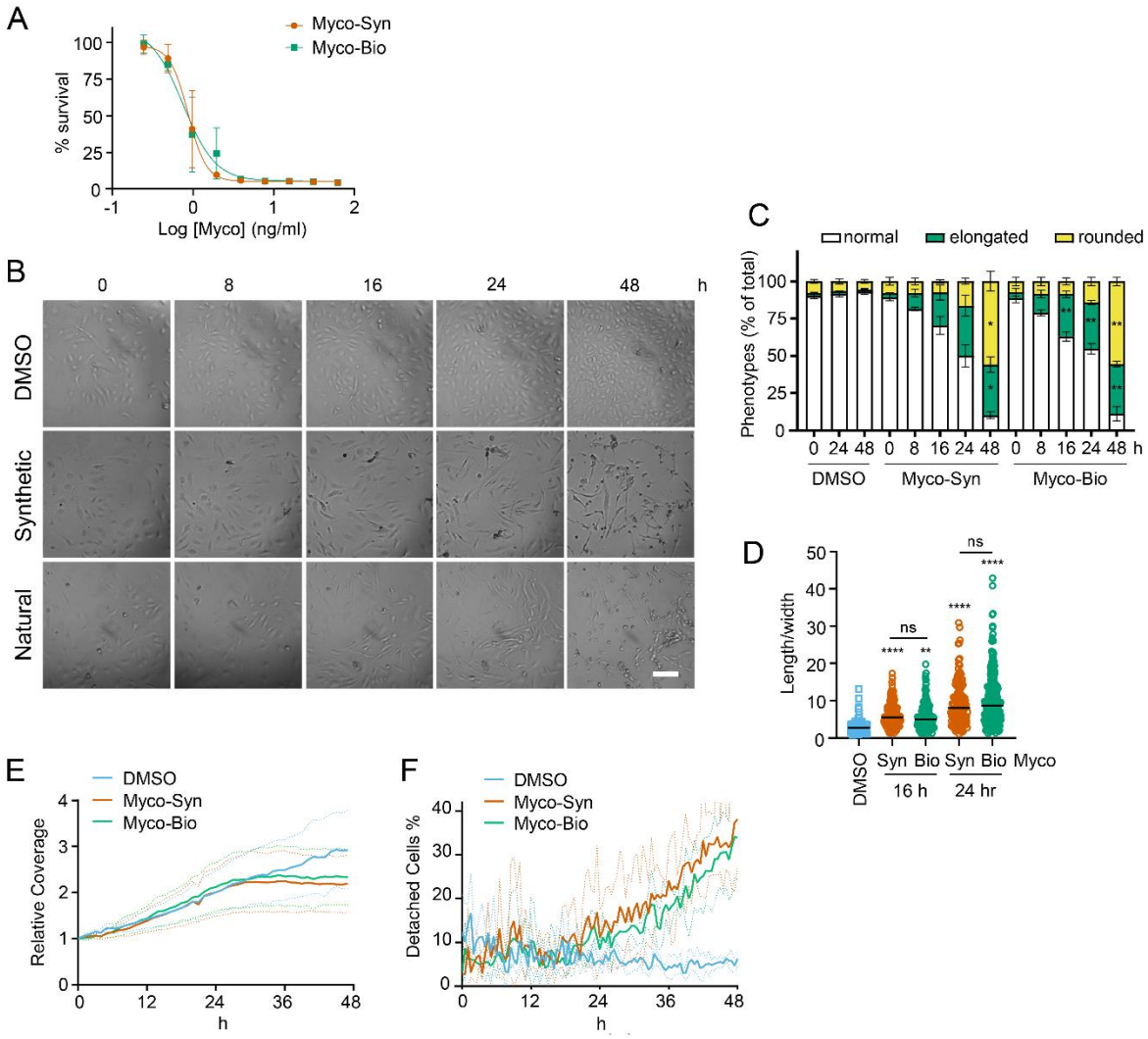

Figure S1. Sec61 inhibition alters endothelial cell morphology. **A.** Dose response of HDMEC to mycolactone produced synthetically (Myco-Syn) or purified from natural sources (Myco-Bio). Cells were exposed in triplicate to serial dilutions of compound for 96hr and viability measured with resazurin. Results are expressed as a percentage of the DMSO control. Data represents the mean of 3 independent experiments ± SEM. **B**. Cells treated with 10ng/ml synthetic (Syn) or natural (Nat) or 0.02% DMSO were imaged using the ZenCELL owl at indicated times. Scale bar =50µ. Images are representative of three independent experiments **C**.Cell numbers of each phenotype were counted and presented as a percentage of total cell number per field in (**B**) (mean ± SD for triplicate wells) *, $p<0.05$; **,$p<0.01$, n=1. **D.** Length and width of cells exposed to mycolactone for 16 and 24 hours or DMSO for 24 hours measured and presented as a ratio. **,$p<0.01$; ****, $p<0.0001$, Data is representative of duplicate independent experiments. **E-F.** Analysis determined by zenCell Owl inbuilt algorithms for images collected over 48hrs of cell coverage (**E**) and detached cells (**F**). Data represents the mean ± SD for triplicate wells, Data is representative of duplicate independent experiments.

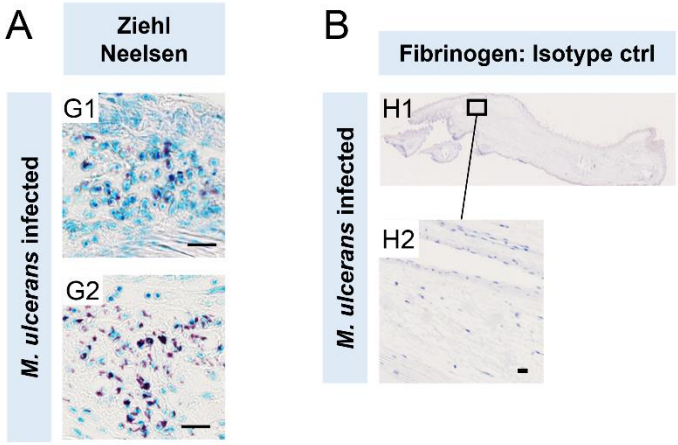

Figure S2. Profile of Buruli ulcer mouse footpad model. C57BL/6 mice receiving $1*10^5$ colony forming units *M. ulcerans* Mu_1082 strain injected intradermally into the footpad were sacrificed at 21or 28 days. Injected feet were fixed, decalcified and embedded in paraffin. (**A**) Sections stained for acid fast bacilli with Ziehl Neelson stain from mice infected for 21 days (A1) or 28 days (A2). At 21 days immune cell infiltration as well as apparently intracellular bacteria can be clearly seen in proximity to mycobacterial clusters (**B**) *M. ulcerans* mouse feet infected stained with isotype control antibody. Scale bars: 20 µm.

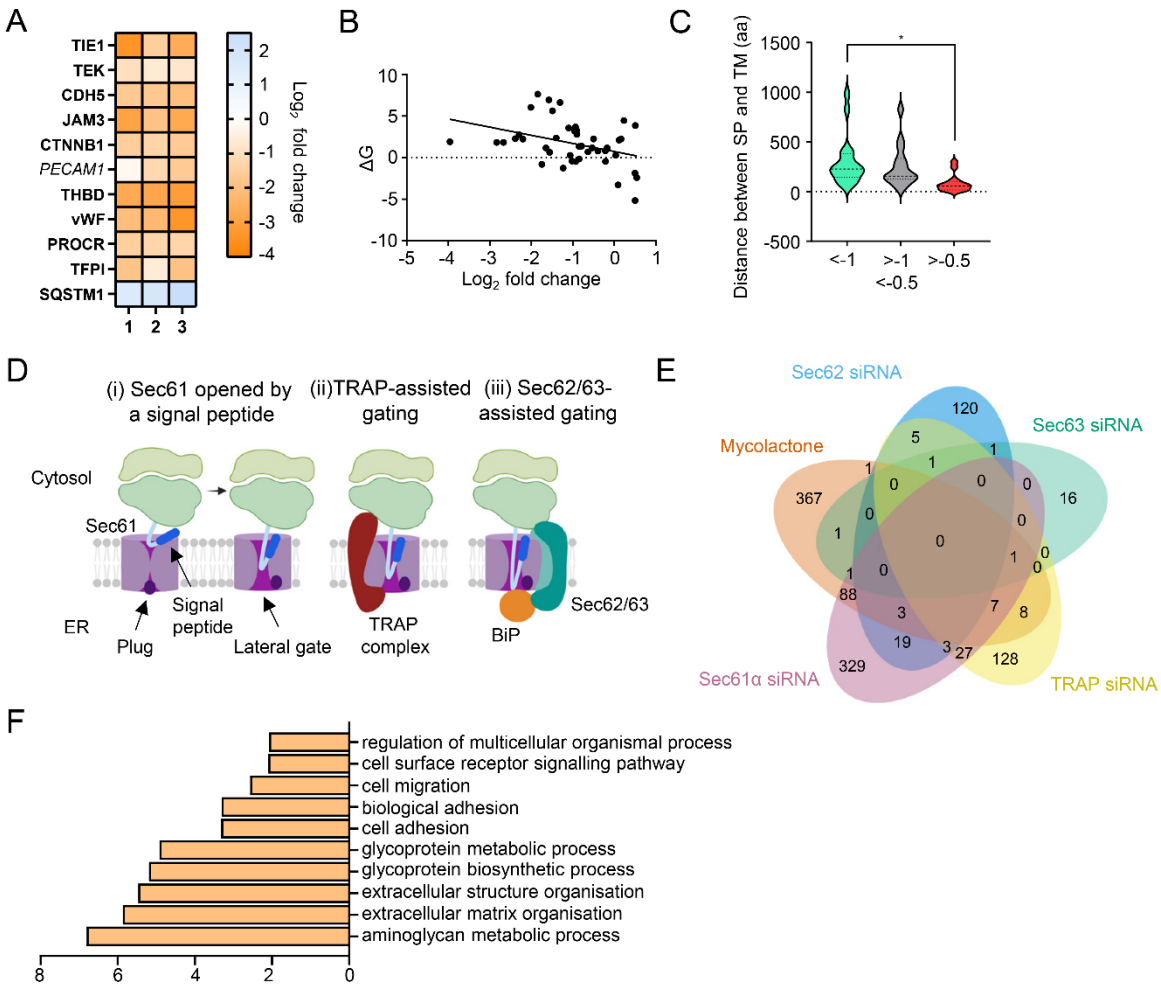

Figure S3. Proteomic analysis reveals loss of proteins associated with glycosylation, adhesion and migration. (**A**) Heat map showing fold change detected in this dataset for previously validated endothelial cell mycolactone targets (Ogbechi et al, 2015, Hsieh et al 2022). Dual-colour coding is shown., significantly downregulated ($p < 0.05$) or not ($p \geq 0.05$) in bold or *Italic* respectively. (**B**) Significant association between multipass protein membrane protein signal peptide (SP) ΔG values and level of downregulation by mycolactone (p<0.05). Membrane protein type and SP sequence based on Uniprot data, ΔG quantified using ΔG Prediction Server V1.0 (https://dgpred.cbr.su.se). (**C**). Impact of distance between signal peptide and first transmembrane domain on susceptibility of multipass proteins to downregulation by mycolactone. Statistical analysis was performed by one-way ANOVA with Tukey's correction for multiple comparisons in GraphPad Prism Version 9.4.1. *, p<0.05 (**D**) Model depicting assisted and unassisted channel opening by signal peptides. (i) Binding of a nascent chain signal peptide to Sec61α opens a lateral gate into the membrane and causes a shift in the position of the plug domain, allowing access to the ER lumen. (ii) TRAP increases translocation of proteins whose signal peptides bear a high GP content. TRAP is a heterotetrameric complex which interacts with the ribosome on the cytosolic side of the ER membrane and with Sec61α on the luminal side, binding to a hinge region between the N- and C-terminal halves of the protein facilitating channel opening [1, 2] (iii) The Sec62/63 complex is involved in post-translational translocation but can also assist opening of the channel for proteins with signal peptides that gate slowly due to the presence relatively long but less hydrophobic "H-regions" and lower carboxy terminal polarity [3]. This complex also interacts with the ribosome and the translocon and may also interact directly with the nascent peptide chain [4]. In addition, Sec63 recruits BiP to the translocon to further assist channel opening on the luminal side [3]. (**E**) Overlap between mycolactone-downregulated endothelial membrane proteome and translocon-dependent proteome. Venn diagram created using JVenn [5] showing overlap in significantly downregulated proteome between the dataset presented here and those obtained in Hela cells treated with siRNA for Sec61α and translocon associated protein TRAP or HEK293 cells with Sec62 or Sec623 knocked out [1, 3]. (**F**) Top significantly over-represented (p<0.05) Gene Ontology groups in upregulated data set, compared to whole genome. Data generated with WebGestalt.

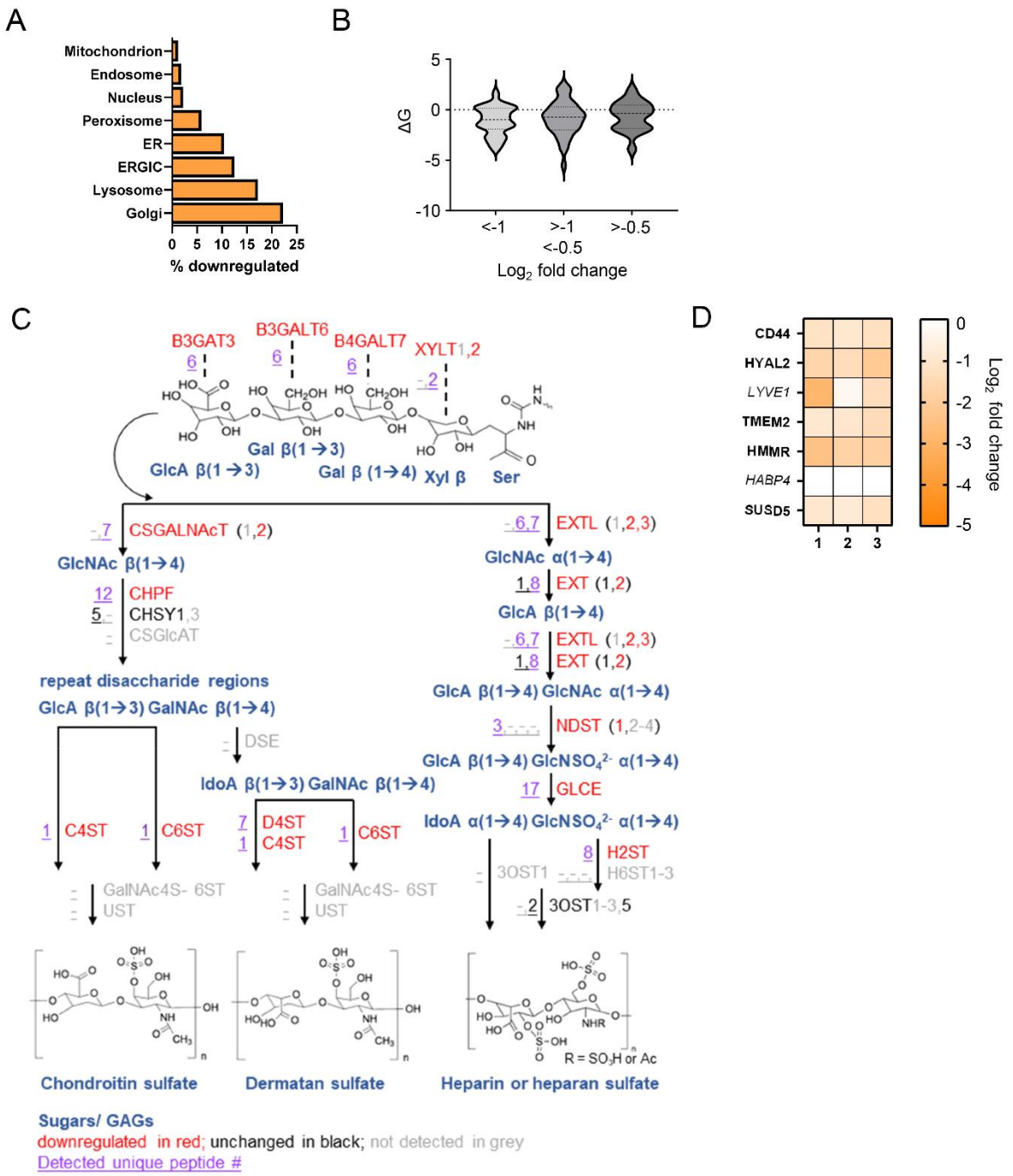

Figure S4. Mycolactone targets Golgi proteins involved in glycosaminoglycan chain synthesis initiation.. **(A)** Downregulated intracellular proteins in HDMECs following 24 hours exposure to 10 ng/mL mycolactone, according to subcellular location, presented as percentage of total. **(B)** Impact of membrane anchor ΔG values on fold change in expression induced by mycolactone for all identified Type II membrane proteins. (**C**) Cartoon representing mycolactone-downregulated steps of GAG enzymatic synthesis. Each intermediate product is shown in blue and alongside with its responsible enzyme(s). Candidates significantly downregulated ($p < 0.05$) by mycolactone are shown in red, unchanged in black and undetected in grey. Unique peptide numbers detected in proteome are in purple (underlined).

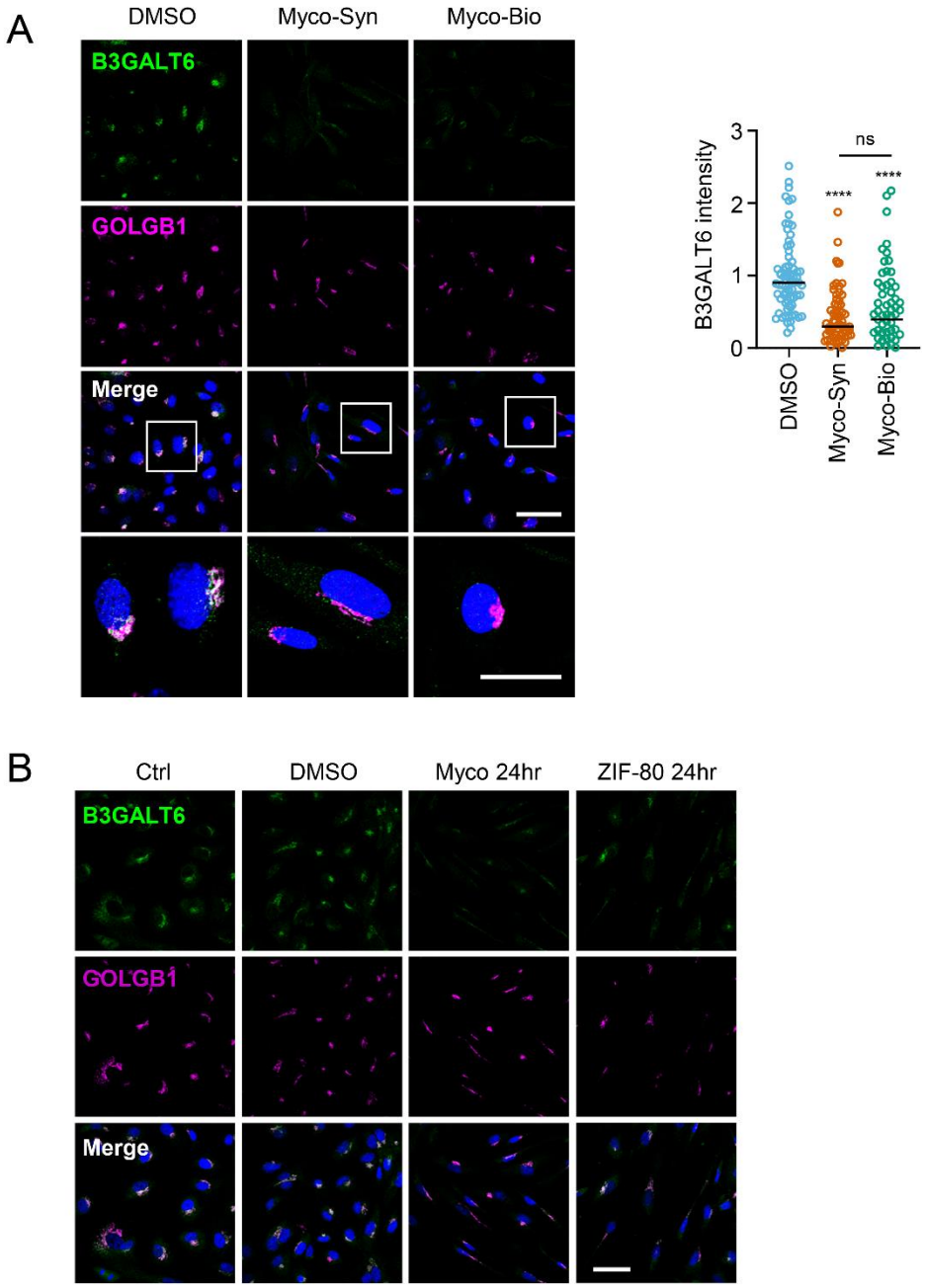

Figure S5. Sec61 blockade suppresses B3GALT6 expression in endothelial cells. A. HDMECs exposed to 10 ng/mL synthetic (Myco-Syn) or natural mycolactone (Myco-Bio) or 0.02% DMSO for 24hr were fixed, permeabilised and immunostained with anti-B3GALT6 and anti-giantin antibodies. **B3GALT6** (green) and the Golgi apparatus (magenta) were visualised and nuclei stained with DAPI (blue). Scale bar = 50 µm (20 µm in the crop panels). Corrected total cell fluorescence of B3GALT6 in Golgi apparatus per cell measured and presented as a value normalised to the mean value obtained from untreated control of each experiment. At least 60 cells per condition were measured. Data is representative of duplicate experiments. ****, $p<0.0001$. (**B**) HDMECs exposed to 10 ng/mL of mycolactone (Myco), 0.02% DMSO, 20 nM ZIF-80 or untreated for 24 hours were fixed, permeabilised and immunostained with anti-B3Galt6 and anti-giantin antibodies and nuclei stained with DAPI. Images are representative of 2 independent experiments. Scale bar = 50 µm. Statistical analysis was performed by one-way ANOVA with Dunnett's correction for multiple comparisons in GraphPad Prism Version 9.4.1

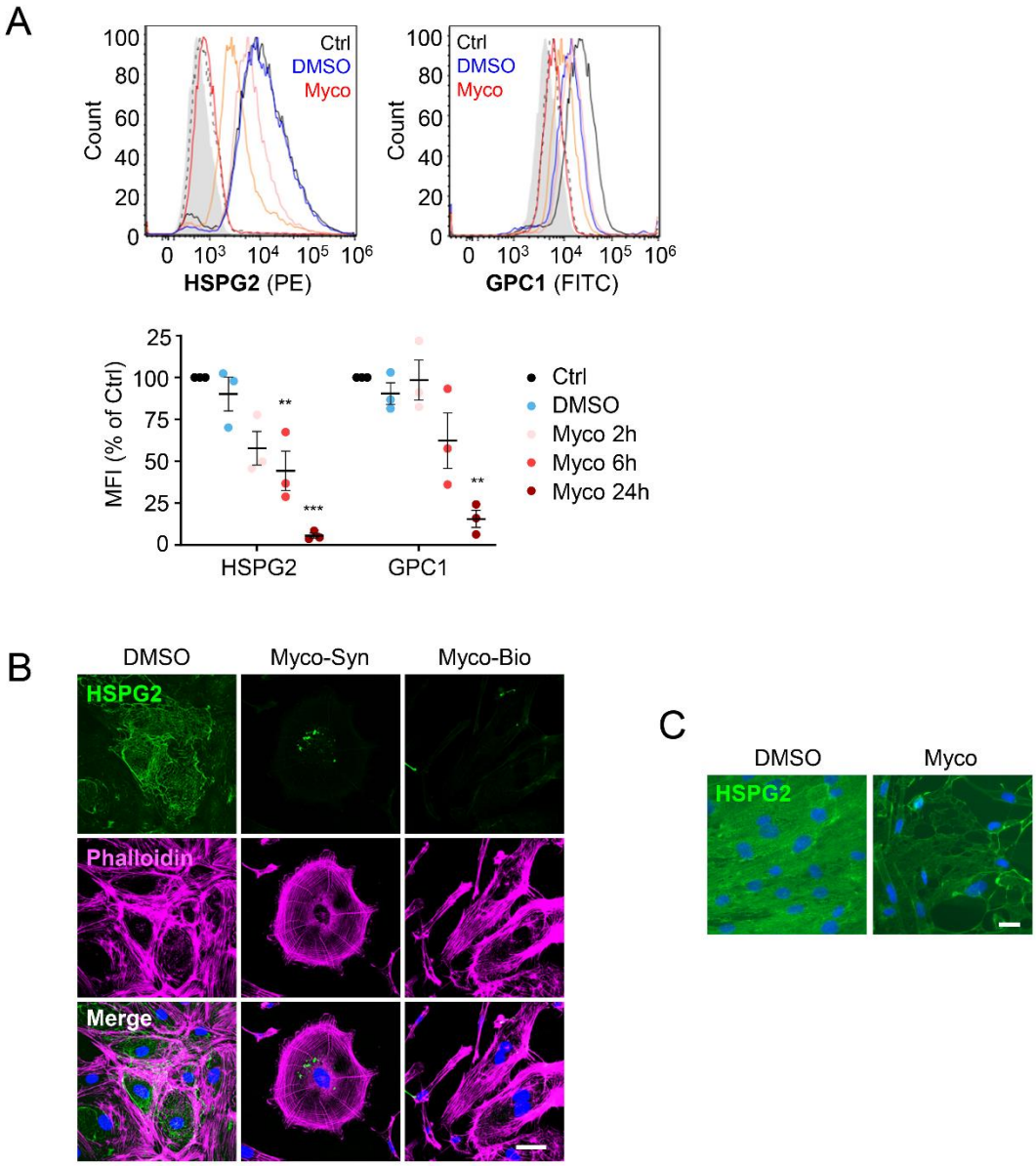

Figure S6. Mycolactone's effect on endothelial surface proteoglycans. HUVECs exposed to 10 ng/mL of mycolactone (Myco), 0.02% DMSO or remained untreated for indicated times. Cells were harvested for flow cytometry analysis. Histogram plots for single cell population of perlecan and glypican-1. Unstained, untreated cells, filled grey; isotype control of untreated cells, dashed black line. untreated cells stained with antibodies, black line; cells exposed to DMSO stained with antibodies, blue line; cells exposed to mycolactone for 2, 6, and 24 hours stained with antibodies, pink, orange and red line, respectively. MFI is presented as a % of untreated control (mean ± SEM of 3 independent experiments). **B**. HDMECs exposed to 10 ng/mL synthetic (Syn) or natural mycolactone (Nat) or 0.02% DMSO for 24 hours. Cells were fixed and immunostained with anti-perlecan antibody (green), permeabilised and labelled with TRITC-conjugated phalloidin (magenta). Nuclei were stained with DAPI (blue). Scale bar = 20 µm, n=1. **C.** Confluent HDMEC incubated on a rotary shaker for 24hr before addition of 0.02% DMSO or 10ng/ml mycolactone (Myco) for 48hr were fixed and stained with anti-perlecan antibody (green) and counterstained with DAPI (blue). Scale bar = 10 µm, n=1.. Statistical analysis was performed by one-way ANOVA with Dunnett's correction for multiple comparisons in GraphPad Prism Version 9.4.1. ns, not significant; **, $P < 0.01$; ***, $P < 0.001$.

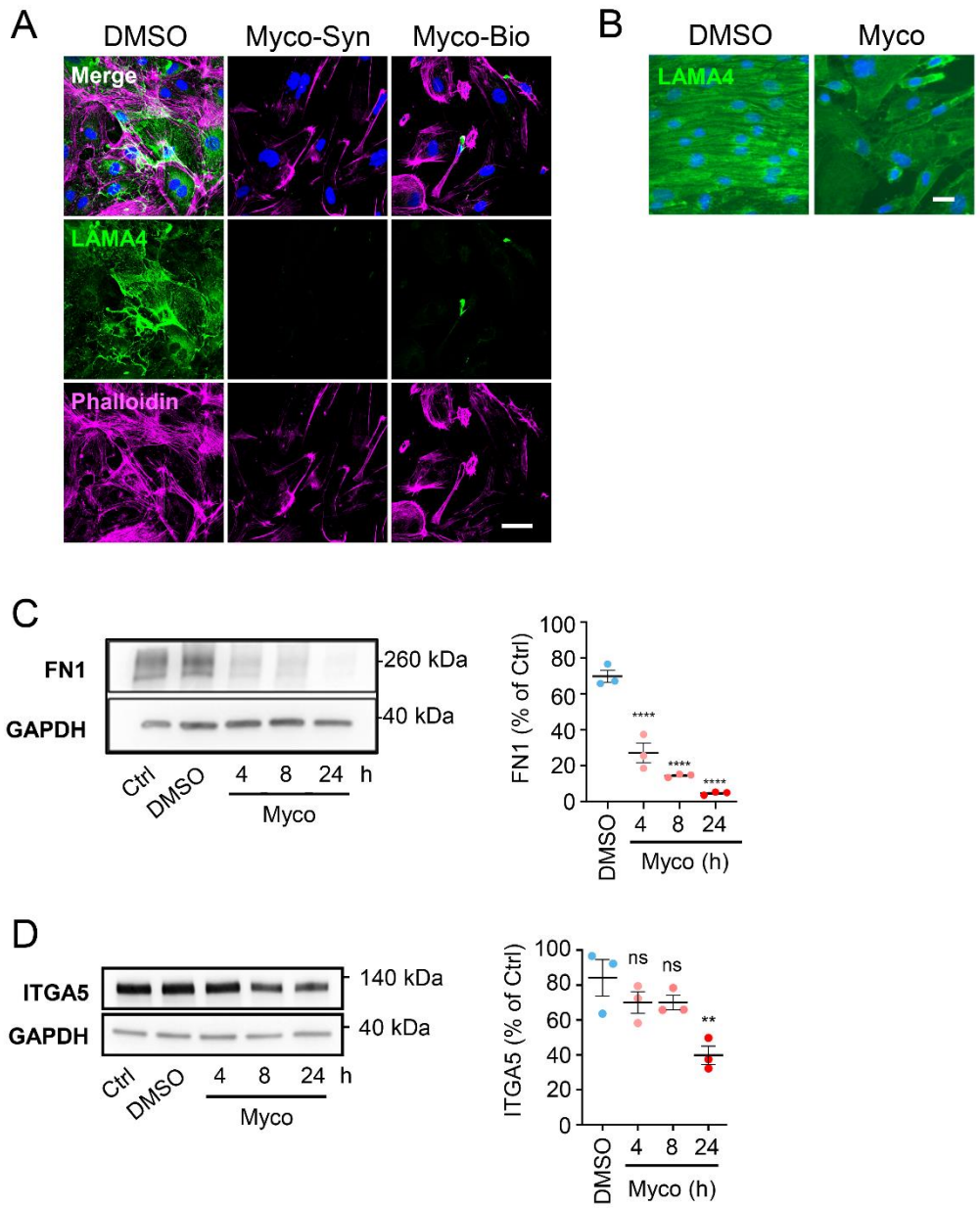

Figure S7. Mycolactone impacts endothelial cell adhesion molecules. A. HDMECs exposed to 10 ng/mL synthetic (Myco-Syn) or natural mycolactone (Myco-Bio) or 0.02% DMSO for 24 hours. Cells were fixed and immunostained with anti-LAMA4 antibody (green), permeabilised and labelled with TRITC-conjugated phalloidin (magenta). Nuclei were stained with DAPI (blue). Scale bar = 20 µm, n=1. **B**. Confluent HDMEC incubated on a rotary shaker for 24hr before addition of 0.02% DMSO or 10ng/ml mycolactone (Myco) for 48hr were fixed and stained with anti-LAMA4 antibody (green) and counterstained with DAPI (blue). Scale bar = 10 µm, n=1. **C-D**. HDMECs exposed to 10 ng/mL of mycolactone (Myco), 0.02% DMSO or remained untreated for indicated times. Cells were lysed and subjected to immunoblotting with anti-fibronectin (**C**) and anti-integrin α5 D) antibodies. Each immunoblot intensity was normalised according to GAPDH and untreated controls. Statistical analysis was performed by one-way ANOVA with Dunnett's correction for multiple comparisons in GraphPad Prism Version 9.4.1Data from 3 independent experiments are presented (mean ± SEM). ns, not significant; **, $P < 0.01$; ****, $P < 0.0001$.

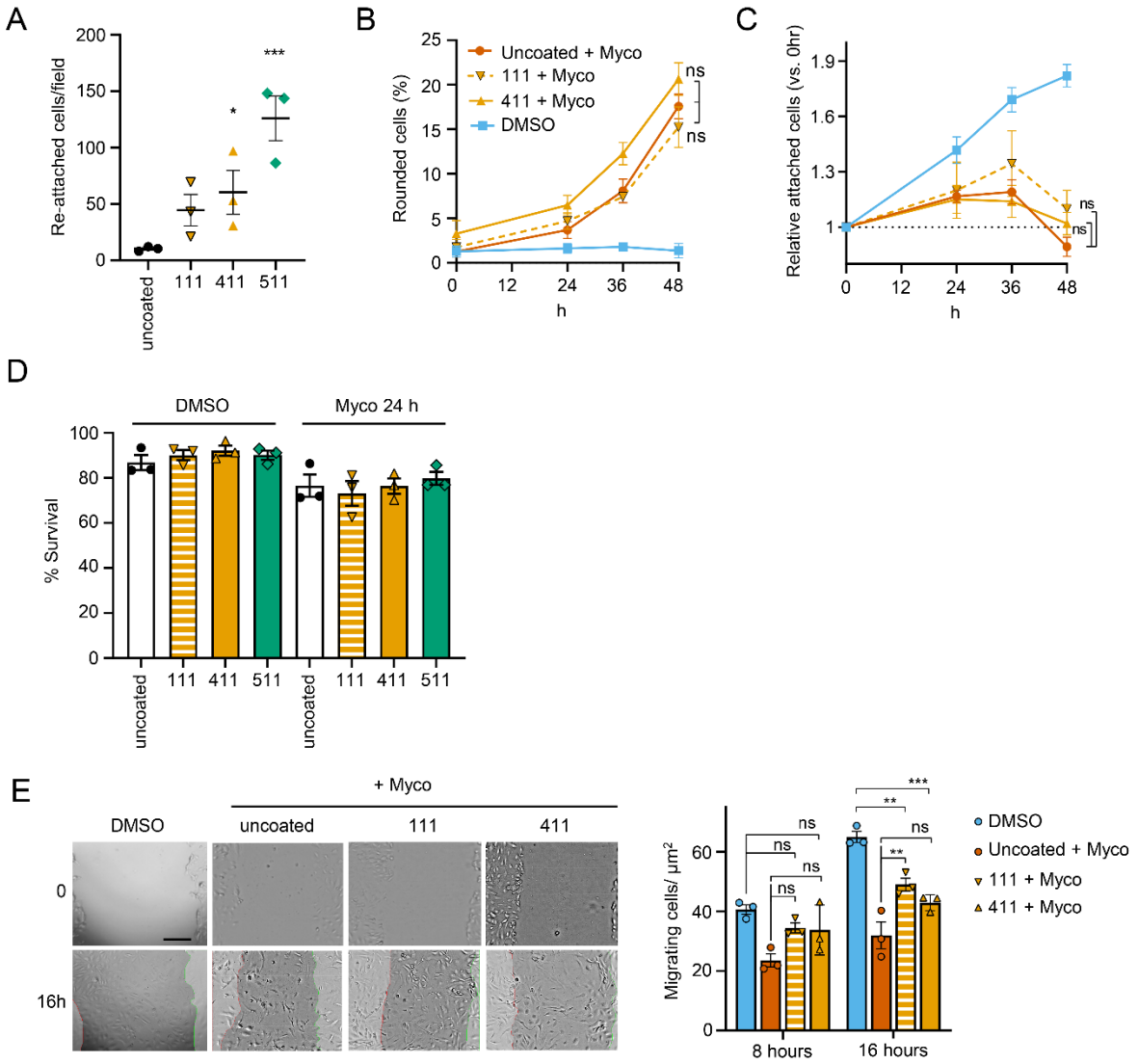

Figure S8. Endothelial cell adhesion to various laminin isoforms. (A) HDMECs were harvested and layered to laminin-511, 411, 111 or uncoated wells for one hour. Non-adherent cells were washed away and attached cells per field were counted. mean ± SEM (n = 3). **(B)** HDMECs seeded onto different laminin isoforms were untreated or exposed to 0.02% DMSO or 10 ng/mL mycolactone (Myco) for 48 hrs. Their viability was assayed using CellEvent detection kit as described in [6]. The number of live cells (negative for both active caspase 3/7 and PI) in three fields was determined and expressed as a proportion of total cells (Mean ± SEM, $n = 3$ independent experiments). Statistical analysis was carried out using GraphPad Prism Version 9.4.1. Panels **A**&**D** used a repeated measures one-way ANOVA with Dunnett's correction for multiple comparisons (**D** also included the Geisser Greenhouse correction for sphericity). Panels **B**,**C**&**E** used a two-way ANOVA with Tukey's correction for multiple comparisons (panels B&C also included the Geisser Greenhouse correction for sphericity). ns, not significant; *, $P < 0.05$; **, $P < 0.01$; ***, $P < 0.001$.

References

1. Nguyen D, Stutz R, Schorr S, Lang S, Pfeffer S, Freeze HH, et al. Proteomics reveals signal peptide features determining the client specificity in human TRAP-dependent ER protein import. Nat Commun. 2018;9(1):3765. Epub 2018/09/16. doi: 10.1038/s41467-018-06188-z.
2. Pfeffer S, Dudek J, Schaffer M, Ng BG, Albert S, Plitzko JM, et al. Dissecting the molecular organization of the translocon-associated protein complex. Nat Commun. 2017;8:14516. Epub 2017/02/22. doi: 10.1038/ncomms14516.
3. Schorr S, Nguyen D, Hassdenteufel S, Nagaraj N, Cavalie A, Greiner M, et al. Identification of signal peptide features for substrate specificity in human Sec62/Sec63-dependent ER protein import. FEBS J. 2020;287(21):4612-40. Epub 2020/03/07. doi: 10.1111/febs.15274.
4. Conti BJ, Devaraneni PK, Yang Z, David LL, Skach WR. Cotranslational stabilization of Sec62/63 within the ER Sec61 translocon is controlled by distinct substrate-driven translocation events. Mol Cell. 2015;58(2):269-83. Epub 2015/03/25. doi: 10.1016/j.molcel.2015.02.018.
5. Bardou P, Mariette J, Escudie F, Djemiel C, Klopp C. jvenn: an interactive Venn diagram viewer. BMC Bioinformatics. 2014;15:293. Epub 2014/09/02. doi: 10.1186/1471-2105-15-293.
6. Ogbechi J, Hall BS, Sbarrato T, Taunton J, Willis AE, Wek RC, et al. Inhibition of Sec61-dependent translocation by mycolactone uncouples the integrated stress response from ER stress, driving cytotoxicity via translational activation of ATF4. Cell Death Dis. 2018;9(3):397. Epub 2018/03/16. doi: 10.1038/s41419-018-0427-y.